NASA
Technical
Paper
2033

January 1983

The Application of Parameter Estimation to Flight Measurements To Obtain Lateral-Directional Stability Derivatives of an Augmented Jet-Flap STOL Airplane

Jack D. Stephenson

NASA

NASA
Technical
Paper
2033

1983

The Application of Parameter Estimation to Flight Measurements To Obtain Lateral-Directional Stability Derivatives of an Augmented Jet-Flap STOL Airplane

Jack D. Stephenson
Ames Research Center
Moffett Field, California

NASA
National Aeronautics
and Space Administration

**Scientific and Technical
Information Branch**

NOMENCLATURE

A	aspect ratio
A_y	lateral acceleration
$a(t)$	state derivative vector
b	wing span
C_J	jet-momentum coefficient
C_L	lift coefficient
C_{L_A}	lift coefficient of airplane wing
C_ℓ	rolling-moment coefficient
C_n	yawing-moment coefficient
C_T	thrust coefficient
C_y	side-force coefficient
D	side-force lag term, $1 - Y_{\dot{v}}$
E	factor $\frac{\rho S b g}{(4W)}$
g	acceleration of gravity
I_x, I_z	moments of inertia about x- and z-axis
I_{xz}	product of inertia
J	cost function (eq. (D24))
J_c	cold thrust
K_v	side slip vane correction factor
$\mathscr{L}, \mathscr{N}$	rolling- and yawing-moment parameters
L, N	rolling- and yawing-moments, transformed variables
N_H	engine speed, % maximum rpm
p	roll rate
$\bar{q}$	dynamic pressure
R_c	ratio of jet-flap chord to wing chord
r	yaw rate

S	wing area
SAS	stability augmentation system
t	time
u,v,w	x-, y-, and z-components of velocity
u(t)	input vector
V	true airspeed
v(t)	measurement noise vector
W	gross weight
w(t)	process noise vector
x(t)	state vector
$\mathcal{Y}$	side force
Y	side force, transformed variable
y(t)	output vector
α	angle of attack
β	angle of sideslip
δ_a	aileron deflection
δ_c	choke deflection
δ_f	landing-flap deflection
δ_R	rudder deflection
δ_s	spoiler deflection
δ_w	control-wheel deflection
δ_{wa}	control-wheel deflection for aileron input
δ_{wb}	control-wheel deflection for spoiler and choke input
$\dot{\delta}$	time-derivative of δ_{wb}
θ	pitch angle
ρ	ambient air density
τ	time; variable of integration

ϕ roll angle

Subscripts:

J due to jet-flap blowing

o without jet-flap blowing

p roll rate

R rudder deflection

r yaw rate

w wing, also control-wheel angle

β sideslip angle

ξ state and control variable

Superscript:

T transpose of vector

Aerodynamic derivatives (referenced to a system of body axes with the origin at the aircraft center of gravity).

$$C_{y_\beta} = \frac{\partial C_y}{\partial \beta} \qquad C_{n_\beta} = \frac{\partial C_n}{\partial \beta} \qquad C_{\ell_\beta} = \frac{\partial C_\ell}{\partial \beta}$$

$$C_{y_{\dot\beta}} = \frac{\partial C_y}{\partial \frac{\dot\beta b}{2V}} \qquad C_{n_{\dot\beta}} = \frac{\partial C_n}{\partial \frac{\dot\beta b}{2V}} \qquad C_{\ell_{\dot\beta}} = \frac{\partial C_\ell}{\partial \frac{\dot\beta b}{2V}}$$

$$C_{y_r} = \frac{\partial C_y}{\partial \frac{rb}{2V}} \qquad C_{n_r} = \frac{\partial C_n}{\partial \frac{rb}{2V}} \qquad C_{\ell_r} = \frac{\partial C_\ell}{\partial \frac{pb}{2V}}$$

$$C_{y_p} = \frac{\partial C_y}{\partial \frac{pb}{2V}} \qquad C_{n_p} = \frac{\partial C_n}{\partial \frac{pb}{2V}} \qquad C_{\ell_p} = \frac{\partial C_\ell}{\partial \frac{pb}{2V}}$$

$$C_{y_w} = \frac{\partial C_y}{\partial \delta_w} \qquad C_{n_w} = \frac{\partial C_n}{\partial \delta_w} \qquad C_{\ell_w} = \frac{\partial C_\ell}{\partial \delta_w}$$

$$C_{y_{\delta_R}} = \frac{\partial C_y}{\partial \delta_R} \qquad C_{n_{\delta_R}} = \frac{\partial C_n}{\partial \delta_R} \qquad C_{\ell_{\delta_R}} = \frac{\partial C_\ell}{\partial \delta_R}$$

THE APPLICATION OF PARAMETER ESTIMATION TO FLIGHT MEASUREMENTS TO OBTAIN LATERAL-DIRECTIONAL STABILITY DERIVATIVES OF AN AUGMENTED JET-FLAP STOL AIRPLANE

Jack D. Stephenson

Ames Research Center

SUMMARY

Tests were conducted to obtain data for calculating the lateral and directional stability derivatives of the Augmented Jet Flap Research Aircraft, an experimental short takeoff and landing (STOL) transport vehicle. The derivatives were calculated using a linear-regression parameter-estimation procedure, with equations of motion of the aircraft represented by a linear model. For the tests reported here, the jet flaps of the airplane were deflected 65°, a typical landing approach configuration. The study included determination of the effects on the derivatives of angle-of-attack variation, the effect of variation in the momentum coefficient of the jet-flap flow, and the effect of varying the angular position of the primary jet-thrust nozzles (located on the engine nacelles). This latter variable could be investigated because the aircraft is designed so that the pilot can control the nozzle angles to vary the thrust direction.

The stability derivatives are compared with predicted values that had been incorporated into a simulation model for the airplane. At all test conditions, the roll damping from the flight measurements was significantly greater than that predicted. Effects on the stability derivatives of varying the momentum coefficient of the jet-flap flow and of varying the primary jet-thrust angle were relatively small. Values obtained for the derivatives C_{ℓ_r} and C_{n_r} were generally in agreement with the predictions. The derivatives C_{n_β} and C_{n_p} agreed with predictions at moderate angles of attack, but their variation with angle of attack differs somewhat from the predictions. Application of a maximum-likelihood parameter-estimation procedure to the flight data yielded average derivative values that are essentially the same as those from the linear-regression solutions; however, for some test conditions there was considerable dispersion in the maximum-likelihood estimates.

INTRODUCTION

The Augmented Jet Flap Research Aircraft was designed and built to provide information on various flight characteristics of a transport aircraft capable of short takeoff and landing (STOL) operations. The flight-test program included maneuvers that would allow the calculation of lateral-directional stability derivatives for the airplane under conditions representing low-speed landing approaches, where, for this type of airplane, handling characteristics are generally inferior to those of conventional aircraft.

Before the airplane was first flown, its flight characteristics had been predicted for use in a simulation model for the Ames Flight Simulator for Advanced

Aircraft (FSAA). This model was based on data from tests of one design version in the Ames 40- by 80-Foot Wind Tunnel and on predictions from theory of some of the stability derivatives. One objective of the present study was to determine the accuracy of such predictions as applied to a configuration employing the augmented jet-flap, powered-lift concept. The study also demonstrates the use of a linear-regression parameter-estimation procedure with a linearized mathematical model for the lateral-directional dynamic behavior of the aircraft; the procedure was used to obtain estimates of stability and control derivatives throughout a range of angles of attack and jet-momentum coefficients. Results obtained by processing some of the data using a maximum-likelihood parameter-estimation procedure are presented, and these results, as they compare with those from the regression solutions are discussed.

THE RESEARCH AIRCRAFT

The Augmented Jet Flap Research Aircraft is a modified high-wing transport powered with two nacelle-mounted jet engines. The engines, in addition to providing direct propulsive thrust, supply bypass air for a system of lift-augmentation jet flaps. This augmentation system is described in references 1 and 2. The engine hot exhaust efflux (providing jet thrust) is directed through nozzles (on the sides of the nacelles) that can be rotated through an angular range from a few degrees below the longitudinal axis of the airplane downward to a position 104° from this axis.

A photograph and a three-view sketch of the airplane are shown in figures 1 and 2, respectively. Figure 3 illustrates some of the details of the flap system and of the lateral control surfaces. The leading-edge slats (fig. 2) are fixed in the extended position. Additional geometric information, weights, and moments of inertia are listed in table 1. A more complete description of the aircraft is presented in references 1 and 3.

The lateral-control system utilizes three aerodynamic surfaces: ailerons with boundary-layer blowing; spoilers located ahead of the ailerons; and in the outer section of each augmentor flap a hinged lower flap element (referred to in this report as the "choke"). When deflected, the choke decreases the lift due to the flap. The lateral-control surfaces are operated through the control wheel by a central dual hydraulic power actuator; the actuator drives one cable system to the ailerons and another to the spoilers and chokes.

Directional control is provided by a two-panel rudder, the aft panel being hinged to the trailing edge of the forward panel and geared to it with a 2:1 deflection ratio. The rudder is fully powered through a hydraulic actuator controlled by cables from the pedals.

In normal operation the aircraft makes use of a lateral-directional stability augmentation system, but for the tests that are the subject of this report, this system was switched off.

The airplane was fitted with a nose boom on which were mounted an angle-of-attack vane, a sideslip vane, and Pitot-static instrumentation. An on-board pulse-code modulation (PCM) data acquisition system provided time-histories of approximately 95 variables at a sample rate of 100 frames per second. In addition to the nose-boom measurements, the recorded data included the following: roll, yaw, and pitch rates; roll and pitch attitude; linear accelerations in three body axes;

ambient conditions; the position of each control surface; engine-performance parameters; and temperatures and pressures in the ducts carrying bypass air to the flap system.

REDUCTION OF DATA

Aerodynamic interference effects were estimated and corrections were applied to airspeed, angle-of-attack, and sideslip data. The airspeed and static pressure errors were determined from tests, using a "pacer" helicopter towing a trailing "airspeed bomb"; the errors are functions of landing-flap angle and aircraft lift coefficient. The angle-of-attack vane error was determined from measurements in steady flight of pitch attitude, longitudinal acceleration, airspeed and altitude (ref. 1). A correction for the induced sidewash due to sideslip was applied to the measurement of sideslip by the nose-boom vane. It was calculated using the equations given in appendix A and data from the maneuvers that are the subject of this report. The actual sideslip angle was determined to be about 18% smaller than the indicated value at angles of attack up to 11°. At higher angles of attack, the correction was slightly larger.

Lateral-control derivatives presented here are derivatives with respect to the control-wheel angle, a variable that represents the combined effects of the three lateral-control surfaces. The wheel angle (in radians) is used in defining these derivatives to permit a direct comparison of the data with predicted control effectiveness used in the simulation model. However, because of the effects of cable stretch and of lags in the actuation system, measured wheel angle was found to be unsuitable as a variable to correlate the aerodynamic characteristics of the lateral control. For this reason, an effective control-wheel angle was defined based on the measured displacements of the control surfaces assuming a linear variation of the wheel angle with displacement. Separate wheel angles are computed for each control. For the ailerons, defining δ_a as the average of the left and right aileron deflection,

$$\delta_{w_a} = 3.62\ \delta_a$$

Spoilers: $$\delta_{w_{SP}} = 1.0\ \delta_{spoiler}$$

Chokes: $$\delta_{w_{CH}} = 3.1\ \delta_{choke}$$

where $\delta_{spoiler}$ is the angular deflection (in degrees) of the spoiler that is deployed; δ_{choke} is the percent closure of the area between the augmentor flap elements; and deflections producing a roll to the left are defined as negative in sign. Figure 4 shows the variations of the lateral-control surface deflections with control-wheel angle (in degrees), measured with no aerodynamic load and for comparison, the effective wheel angles given by the above relations.

The directional control deflections are computed using the rudder angle, measured in degrees, on the forward rudder panel.

The efflux of engine bypass air from nozzles at the augmented jet flaps produces aerodynamic effects that are correlated on the basis of a jet-momentum coefficient C_J. This coefficient — equal to $J_c/(\bar{q}S)$, where J_c is the ("cold") thrust due to

the ejected air — is computed from engine static test data and flight measurements of engine rpm, ambient air conditions, and internal duct temperatures and pressures. A jet-momentum coefficient, based on the thrust calculated assuming isentropic expansion of the bypass air flow to static ambient pressure, was determined to be about 32% larger than C_J defined above at all conditions for which results are presented.

The engine direct ("hot") thrust (T) and a thrust coefficient C_T ($C_T = T/(\bar{q}S)$) were also obtained from engine static test data and from flight-measured engine and environmental information. Figure 5 shows, as functions of engine percent rpm, the thrust coefficient and the ratio C_J/C_T for an equivalent airspeed of 70 knots and standard atmospheric conditions, at two altitudes, 610 M (2,000 ft) and 1,830 m (6,000 ft).

FLIGHT EXPERIMENTS

Data analyzed in this report were obtained from maneuvers produced by control-wheel and rudder inputs approximating doublet functions. During the maneuvers, the pilot attempted to maintain either a constant airspeed or a constant angle of attack. To perform the maneuver, he established the specified initial conditions in wings-level steady flight, applied the control input, and then, with the rudder and lateral controls centered, allowed the motion to continue through two to three cycles of Dutch roll.

The flight experiments were conducted at various times as scheduling permitted throughout an extended period of time when the aircraft was also being flown for a variety of other research purposes. Results of the earlier tests revealed some details of the execution of the maneuvers that affected the quality of the data. For example, with maneuvers produced by a control-wheel input, a large maximum angular displacement of the wheel (greater than about 25°) yielded better quality data than maneuvers that were performed with small wheel excursions. In the same type of maneuver, even a small movement of the rudder had significant adverse effects.

All of the tests were performed with the lateral-directional stability augmentation system switched off; and without stability augmentation, the handling characteristics of the aircraft are poor, particularly at the lowest airspeeds used in the tests. As a result, performance of the tests conducted later in the program improved as the pilots became more familiar with the flight characteristics of the aircraft. In addition to maintaining approximately constant speed, a satisfactory maneuver usually required that the Dutch roll response be relatively symmetrical about a wings-level attitude, avoiding a tendency toward roll divergence.

In all of the tests from which data were obtained in this program, the augmented jet flaps were set at a deflection of 65°, a typical setting for landing approach. With this flap setting the ailerons have 30° droop. Tests were planned to cover a large angle-of-attack range below stall and a range of engine thrust levels up to the maximum engine rpm specified for continuous operation. To determine the effects of thrust vectoring and interactions of the jet efflux and the external airstream, tests were conducted with the thrust nozzles at three settings: their position for takeoff and cruise, that is 8° downward from the fuselage axis; fully down at an angle that was about normal to the flightpath (80° to 90° from the reference axis); and at an intermediate angle of about 60°.

At the outset of the flight program, it was believed that the maneuvers generated by the lateral-control input alone would be sufficient to provide most of the data for extracting the rotary and sideslip stability derivatives. However, in some instances the parameter-estimation calculations resulted in considerable dispersion in estimated parameter values. This was apparently largely a result of inadequate excitation of the yawing motion. It was concluded that maneuvers generated by a rudder input would also be needed — not only for obtaining rudder effectiveness data — but also for use with the calculations of the other derivatives.

A smaller number of maneuvers were performed in which both a rudder and a wheel input were employed. In these, the pilot (1) applied a rudder doublet; (2) continued with a control-fixed Dutch roll, as in the other tests; and (3) then reestablished the initial conditions and applied a wheel doublet. Data were recorded through a second Dutch roll. A typical set of time-histories from one of these maneuvers is illustrated in figure 6.

STABILITY-DERIVATIVE PREDICTIONS

Predicted lateral-directional stability and control characteristics, which furnish part of the information used to develop a simulation model for the research aircraft, were derived from wind-tunnel tests and theory and from semiempirical rules, such as those discussed in references 4 and 5. A large-scale model having an augmented jet flap and other design features similar to those of the airplane was tested in the Ames 40- by 80-Foot Wind Tunnel (refs. 6 and 7). Static stability derivatives and lateral-control effectiveness predictions were based on these tests, with appropriate modifications to account for differences in the areas of the various (control and flap) surfaces.

A method for calculating lateral-directional rotary derivatives from theory for a wing with a jet flap is developed in reference 8. An extension of this work by J. Farbridge of de Havilland Aircraft of Canada, applicable to the Augmented Jet Flap Research Aircraft configuration, is outlined in appendix B. This provides a calculated contribution of the wing that, when combined with the estimated contributions of the other aerodynamic components, furnished the expressions that were used to obtain the rotary derivatives for the simulation model of the complete configuration. These expressions and those for the static stability derivatives are given in appendix C; they are reproduced from reference 9, which describes the simulation model in detail, and includes predicted lateral and directional control characteristics. The control characteristics are in tabular form and are generally nonlinear. However, within the range of rudder deflections used in the tests reported herein, the predicted rudder characteristics are very nearly linear with deflection angle.

Possible effects of the direct hot thrust and the thrust-vector angle on the lateral-directional stability derivatives were neglected in these predictions.

EXTRACTION OF THE STABILITY DERIVATIVES

The lateral-directional stability and control derivatives were calculated from time-history records of the flight maneuvers, using the parameter-estimation procedure described later in this section. The application of parameter-estimation methods to extract stability derivatives has been discussed and demonstrated in many reports

(refs. 10-15). In these procedures, a mathematical model, assumed to represent the dynamic behavior of the flight vehicle, generates a response to an input that is a measurement of the pilot's control input. The parameter-estimation calculations attempt to determine the set of parameter values for the model that for this input causes the model response to best match the measured response.

The following equations are assumed to represent the lateral-directional dynamics of the aircraft in the body-axis system; I_x and I_z are the aircraft moments of inertia about the x and z axes, I_{xz} is the product of inertia, and a dot over a variable denotes a time-derivative. The equations are for a rigid airplane, assuming no excitation of the longitudinal dynamics (ref. 13):

$$\dot{v} = wp - ur + g \cos \theta \sin \phi + A_y \tag{1}$$

$$\dot{r} = (I_{xz}/I_z)\dot{p} + \mathscr{N} \tag{2}$$

$$\dot{p} = (I_{xz}/I_x)\dot{r} + \mathscr{L} \tag{3}$$

$$\dot{\phi} = p + r \cos \phi \tan \theta \tag{4}$$

In these expressions, u, v, and w are the components of the true airspeed in the x-, y-, and z-direction; p and r are the roll and yaw rates; θ is the pitch angle; and ϕ is the roll angle. Lateral acceleration A_y and the yawing- and rolling-moment terms ($\mathscr{N}, \mathscr{L}$) can be represented by the following relations:

$$A_y = \sum \mathscr{Y}_{\xi_i} \xi_i + \mathscr{Y}_o \tag{5}$$

$$\mathscr{N} = \sum \mathscr{N}_{\xi_i} \xi_i + \mathscr{N}_o \tag{6}$$

$$\mathscr{L} = \sum \mathscr{L}_{\xi_i} \xi_i + \mathscr{L}_o \tag{7}$$

The terms $\mathscr{Y}_{\xi_i}$, $\mathscr{N}_{\xi_i}$, and $\mathscr{L}_{\xi_i}$ are the dimensional side-force, yawing moment, and rolling-moment derivatives, and the ξ_i terms denote the variables v, r, p, $\dot{v}$ and the control variables defined below. The terms $\mathscr{Y}_o$, $\mathscr{N}_o$, and $\mathscr{L}_o$ are the measurement bias terms. With the approximations and substitutions given in appendix D, the state equations can be written as follows.

$$\begin{bmatrix} \dot{v} \\ \dot{r} \\ \dot{p} \\ \dot{\phi} \end{bmatrix} = \begin{bmatrix} Y_v & Y_r - u & Y_p + w & \bar{G} \\ N_v & N_r & N_p & \overline{ND} \\ L_v & L_r & L_p & \overline{LD} \\ 0 & \tan \theta & 1 & 0 \end{bmatrix} \begin{bmatrix} v \\ r \\ p \\ \phi \end{bmatrix} + \begin{bmatrix} Y_{wa} & Y_{wb} & Y_{\dot{\delta}} & Y_R \\ N_{wa} & N_{wb} & N_{\dot{\delta}} & N_R \\ L_{wa} & L_{wb} & L_{\dot{\delta}} & L_R \\ 0 & 0 & 0 & 0 \end{bmatrix} \begin{bmatrix} \delta_{wa} \\ \delta_{wb} \\ \dot{\delta} \\ \delta_R \end{bmatrix} + \begin{bmatrix} Y_o \\ N_o \\ L_o \\ 0 \end{bmatrix} \tag{8}$$

in which the parameters represent the dimensional derivatives after applying the transformations in appendix D, equations (D7) and (D10) through (D14). The angle θ is the constant time-averaged value of the measured pitch attitude during the maneuver. Also, u and w, the axial and normal components of velocity, are assumed to

to be constant and are given by the following relations in which V_{av} and α_{av} are the average speed and angle of attack:

$$u = V_{av} \cos \alpha_{av} \qquad w = V_{av} \sin \alpha_{av}$$

Also in equation (8), $\bar{G}$ is the product $g \cos \theta$, and the parameters $\overline{ND}$ and $\overline{LD}$, defined by equations (D12) and (D14), result from inclusion of $\dot{v}$ as a variable to account for aerodynamic forces at the tail that are produced by sideslip-induced sidewash. They were estimated separately (by methods described in ref. 5) and entered as fixed values in the equations.

The displacements of the lateral control surfaces are included as two inputs, both defined as effective control-wheel angles. One, δ_{wa}, is calculated from the aileron deflection, and the other, δ_{wb}, is the average of wheel angles computed from the spoiler and the choke deflections. These latter two sets of surfaces moved essentially together but lagged behind the aileron motion. When two inputs were used to model the lateral-control displacement instead of a single input representing the control-wheel displacement, the computed responses consistently showed better agreement with measured time-histories. However, the lag of the second input was too small to permit the estimation of its separate contribution, and so fixed values were entered for one of each of the two lateral input parameters, usually for Y_{wb}, N_{wa}, and L_{wb}. The values of the lateral-control derivatives shown in the figures in this report were obtained by summing the fixed and the extracted values. The third input variable, $\dot{\delta}$, is the time-derivative of δ_{wb}, the spoiler-choke displacement, and is included to take into account an effect of induced flow at the tail caused by changes in circulation resulting from deflection of the lateral control surfaces. The fourth input, δ_R, denotes the rudder displacement.

Parameter Estimation

A parameter-estimation program developed by R. Bach (at Northeastern University and Ames Research Center) was used to obtain the results presented here. The program is described in reference 16, part of which is reproduced in appendix D. It includes a provision for selecting a linear-regression or a maximum-likelihood computational procedure. The regression solution fits linear combinations of measured states to state derivatives and assumes that the state measurements are noise-free. This solution required roll and yaw angular acceleration records, $\dot{p}$ and $\dot{r}$, in addition to the lateral acceleration, A_y, that was measured. The angular accelerations were calculated as the slopes of the curves representing least-squares fits to the roll and yaw rate time-histories.

The maximum-likelihood solution, with state estimation, utilizes a parameter-initialization scheme to obtain a first approximation for the response of the airplane to the control inputs. Then, in successive steps, the solution iteratively varies the parameters to produce a progressively better match of the computed and measured responses. Improvement in the matching of the responses in each step is expressed as a decrease in an error index, or "cost function," J, defined by equation (D24) in appendix D.

It can be shown that linear-regression methods will cause a bias in parameter estimates as a result of measurement noise (see ref. 13). A comparison of results obtained with the two procedures, regression and maximum likelihood, offers an indication whether such a bias is significant in the present experiments. Evidence

presented here indicates that this bias is small. In addition, the linear-regression solution yielded parameter estimates that consistently displayed less dispersion than those from the maximum-likelihood solution that was employed. For this reason, the linear-regression solution was used to obtain most of the results presented in this report. Some comments on the nature of the deviations in the estimates produced by the maximum-likelihood procedure are included in the discussion of results.

To process the data, the time-history records of the variables were sampled at a selected rate, usually at 50 frames per second (i.e., half the rate at which they were recorded) and then, with a filtering routine, the number of data points per variable was further reduced to conform to a program array size limitation of 300. A constant bias was applied to each measurement to set all of the initial values to zero. The parameter-estimation solutions yield estimates of the matrix elements in equation (8). Equations (D15) and (D16) (appendix D) were then used to convert these estimates to the nondimensional stability derivatives shown in the figures that present the results.

Sidewash Due to Sideslip

As mentioned above, the mathematical model for the aircraft motion, equations (1) through (7), includes the variable $\dot{v}$ to account for an effect of induced sidewash in the region of the tail. Stability derivatives with respect to this variable were not estimated, but as the derivation in appendix D shows, its presence can influence the estimated values of the other derivatives. All of the derivative values from the tests (but not the predicted values) include incremental contributions due to this induced sidewash effect. The magnitude of these increments has been calculated, based on predicted values of the $\dot{\beta}$ derivatives given in appendix C (from ref. 9). These are listed in appendix E for three sets of flight conditions corresponding to angles of attack of 2° (90 knots), 7° (75 knots), and 12° (65 knots). The incremental changes are all quite small, except for yaw damping, C_{n_r}. If C_{n_r} is corrected by the amount shown, the yaw damping is reduced by between 6 and 9%, depending on the test conditions and on the actual value of C_{n_r} within the range of deviation of the experimental results.

RESULTS

Stability Derivatives

Figures 7 through 9 present the lateral-directional stability derivatives as functions of angle of attack. As indicated in the figure legends, the various symbols correspond to different ranges of the jet-momentum coefficient, C_J. The solid symbols are results from maneuvers in which the pilot applied a rudder-doublet input followed by a control-wheel doublet. Flagged symbols identify results of calculations in which it was necessary that two of the rotary derivatives be preset at fixed values. The fixed values have been plotted with a smaller symbol size than the computed values. Most of these results are from tests produced by rudder doublets, for which L_p and N_p were fixed. The remaining sets of flagged symbols represent a small fraction of the tests produced by control-wheel doublets, for which the calculations were done with L_r and N_r set at fixed values.

Figure 7 shows results for the configuration in which the engine propulsive thrust nozzles are at an angle of 8° from the fuselage longitudinal axis; figure 8 is

for a 60° angle, and figure 9 is for angles in the range from 80° to 90°. The side-force derivatives, C_{y_p}, C_{y_r}, and C_{y_β} (figs. 7(c), 8(c), and 9(c)), are all from control-wheel maneuvers. These derivatives from the rudder-excited maneuvers displayed excessive dispersion and are omitted.

Figures 7 through 9 show, in addition to the experimental results, solid-line curves representing (at two values of C_J, 0.1 and 0.4) the values for the derivatives that were predicted and used in the simulation model, as discussed in the section on stability-derivative predictions. The predicted values for C_{ℓ_β} and C_{y_β} are independent of C_J.

Lateral and Directional Controls

Rolling-moment, yawing-moment, and side-force derivatives with respect to the control-wheel angle are shown in figure 10. As described in the section on reduction of data, the control-wheel angle used to define these derivatives is calculated from the measured displacements of the lateral-control surfaces, with gearing ratios from ground calibrations. Also shown in the same figures are the derivatives with respect to the rate of displacement of the lateral control. As indicated in the discussion of the mathematical model for the aircraft dynamics, these derivatives are included to account for forces and moments that result from downwash and sidewash (at the tail) induced by the lateral-control deflection.

In figure 11, rolling-moment coefficients are shown as a function of control-wheel angle. The two solid-line curves are predictions used in the simulation model, based on large-scale wind-tunnel tests, for two values of C_J, 0.1 and 0.35. The cross-hatched region corresponds to the results from the parameter-estimation program, which yields the slopes of linear curves through the origin. The region shown was obtained by averaging the results of all tests for which the average angle of attack was in the range from 2° to 10°, its width being computed as twice the standard deviation.

Figure 12 shows the directional control characteristics. These are the derivatives with respect to the rudder-deflection angle measured (in degrees) on the forward panel of the two-panel rudder. The rudder characteristics used in the simulation model are shown as the solid-line curves and apply to a range of rudder-deflection angles within which the predicted variation is linear, that is, up to about 15°. For the flight experiments, the deflections were within this range.

DISCUSSION

The test results (figs. 7-9) indicate that the magnitude of the roll-damping derivative (C_{ℓ_p}) is significantly greater than that used in the simulation model and that at angles of attack near zero, it varies more rapidly with angle of attack than predicted. The large estimated roll damping indicates that the section lift-curve slopes for the outer portions of the wing are relatively high. The usual deleterious effects of large aileron and spoiler deflection on lift-curve slopes appear to be alleviated by boundary-layer blowing at the aileron and by the leading-edge slat configuration that is used.

The graphs of C_{ℓ_β} show a large dihedral effect at small and negative angles of attack and a gradual decrease in this effect as the angle of attack becomes large. The curves representing the predicted C_{ℓ_β} are based on wind-tunnel measurements and indicate values near zero for all conditions. The wind-tunnel model had no geometric dihedral, whereas the flight vehicle was constructed with a 5° dihedral in the wing panels outboard of the engine nacelles. The graphs showing C_{n_β} indicate a decrease in this derivative with angle of attack, compared with a predicted constant value, but the levels at moderate angles of attack are in agreement. The levels of yaw damping and the derivative C_{ℓ_r} generally agree with predictions; C_{n_p} is in agreement at small angles of attack but shows a somewhat greater rate of variation with angle of attack.

Side-force data plotted in figures 7(c), 8(c), and 9(c) indicate that the values of derivatives C_{y_p} and C_{y_β} are near the predicted levels; there is little variation of C_{y_β} with angle of attack, although a negative variation was predicted. The average of the estimates for C_{y_r} is larger than predicted by 30% to 40% at moderate angles of attack and by over 80% at angles above 8°.

Among all of the derivatives shown in figures 7-9, little or no consistent effect of variation of jet-momentum coefficient C_J is evident. Also for all the derivatives, there is significantly more dispersion in the estimates from tests in which the engine thrust nozzles were at angles in the range from 80° to 90° than for the smaller angles (8° and 60°). At angles of attack where comparisons can be made, the effects on the derivatives of changing the angles at which the nozzles were set appear to be small.

Figure 10(a), which shows the lateral-control effectiveness C_{ℓ_w} for the configuration with the engine thrust nozzles at 8°, indicates an increase in effectiveness with angle of attack. With the nozzles at 60° and 80° to 90°, a consistent effect of angle of attack is not apparent. For all of the nozzle angles, the roll-effectiveness data show little consistent effect of variation of C_J.

From the graphs showing the lateral-control rate derivatives (fig. 10), it is seen that the estimated values of the yawing-moment derivative C_{n_δ} are predominently negative in sign. This can be interpreted as indicating that a positive lateral-control deflection induces a sidewash at the vertical tail, causing an added, but delayed, positive yawing moment. Estimated values for the rolling-moment derivative C_{ℓ_δ} are also mostly negative in sign. This means that part of the rolling-moment response to the lateral control is delayed, an effect that can be attributed to an induced downwash that varies along the span of the horizontal tail, with its strength increasing toward the right for a positive control deflection.

Rolling Moment versus Wheel Angle

In figure 11 (rolling-moment coefficient plotted as a function of control-wheel angle), the data from parameter-estimation calculations (the cross-hatched region) represent results from 38 maneuvers covering a range of C_J from 0.1 to 0.38. As mentioned earlier, there was no consistent correlation of C_{ℓ_w} (the slopes of the

curves represented by this region) with this C_J variation. This differs from the predicted effect of C_J, illustrated by the solid line curves in figure 11, where there is a large increase in effectiveness with an increase in C_J from 0.1 to 0.35. The results from the flight experiments indicate a considerably greater rolling moment due to control deflection than that predicted for the smaller C_J. The flight results also show larger rolling effectiveness than predicted for C_J of 0.35 at the larger control-wheel angles. The broken-line curve shown in figure 11 represents rolling-moment coefficients calculated from data reported in reference 3; the data were obtained from roll-reversal maneuvers, in which the roll acceleration was determined at times when the roll rates were near zero. These results indicate a somewhat larger roll effectiveness than that from the parameter-estimation calculations for control-wheel angles in the range from 20° to 40°; at smaller and larger wheel angles, however, the results from the two techniques are generally in agreement. The parameter-estimation results are from maneuvers that were generated by applying a wide range of control-wheel time-history functions. The maximum control-wheel angles used for these input functions ranged from 13° to 62°. For approximately half of the maneuvers, the maximum wheel angles were greater than 40°, and the average of the maximum wheel angles for all of the tests was 37°.

Rudder Effectiveness

As determined from the flight experiments, the yawing moment produced by the rudder (fig. 12) agrees well with that used in the simulation model. The average values for the rolling-moment and side-force derivatives from these tests are about 30% smaller than those in the simulation model. In reference 9, a relation between $C_{n_{\delta R}}$ and $C_{y_{\delta R}}$ is obtained by assuming that the rudder yawing moment is equal to the product of the side force and the distance from the aircraft center of gravity to the aerodynamic center of the vertical tail. The data from the flight experiments indicate that the rudder contributes a significant additional yawing moment attributable to an aerodynamic couple on the vertical tail.

Maximum-Likelihood Results

In figure 13, stability-derivative estimates obtained using the maximum-likelihood solution (appendix D) are compared with estimates from the linear-regression solution. These results are all from flight maneuvers in which the pilot first applied a rudder doublet and then a control-wheel doublet. Data represented by the plain symbols are those shown earlier (with solid symbols in figs. 7-9) from linear regression, and the flagged symbols are from the maximum-likelihood computation. As before, the various symbols correspond to different C_J ranges. A notable difference in the results obtained with the two computational procedures is the increased dispersion in the maximum-likelihood data. The increase is moderate in the results for the aircraft configuration in which the vectored thrust nozzles were at 8° and 60° (fig. 13(a)) and is quite large for the 85° nozzle angle (fig. 13(b)).

It is generally recognized (and shown, for example in ref. 17) that there will be biased estimates resulting from linear-regression solutions, if measurement noise has an important effect. Some indication of such biases can be discerned from figure 13, although scatter in the data prevents an accurate evaluation of their magnitudes. The regression solutions yield slightly larger values for C_{n_β} and indicate slightly less roll damping than the maximum-likelihood solutions, but these differences are quite small. Because of this small effect and because using linear

regression not only resulted in significantly less scatter but also entailed considerably less computer execution time, it is clearly the preferred method for processing the data from the tests reported here.[1] Situations exist, however, in which the maximum-likelihood method with state estimation might be chosen instead; for example, when measurements of all the states are not available, or when measurement noise is so large that it causes significantly biased estimates. For the maximum-likelihood procedure to offer a suitable alternative, it is important that the large dispersion be reduced. A reduction in this scatter was achieved by some minor changes in the way the computations were handled, as discussed below.

The comments that follow are based on the results of applying the maximum-likelihood procedure to all of the relatively large number of time-history records that are the subject of this report. The largest deviations in the parameter estimates were not random in nature. It was evident that when these deviations occurred, an apparent error in one parameter was related to errors in one or more other parameters. In some cases, such correlated errors can be traced to the fact that during the latter part of the maneuvers, when the motion of the airplane is a control-fixed Dutch roll, the side velocity, roll rate, and yaw rate are linearly related. For such motion, errors in one of the three derivatives C_{ℓ_p}, C_{ℓ_r}, and C_{ℓ_β} (or C_{n_p}, C_{n_r}, and C_{n_β}) are compensated for by errors in the other two, with the result that the solution will not necessarily converge to the correct parameter values. Presumably, because of the presence of random perturbations of the aircraft's motion caused by turbulence, the earlier portion of the maneuver does not contribute strongly enough to assure a unique solution. By fixing the value of one of the three derivatives at its correct value, these errors in the other derivatives are minimized. When errors of this type were evident in the results from maneuvers generated by a rudder doublet followed by a control-wheel doublet, better results were obtained by dividing the data records into two time intervals and treating them as separate maneuvers. A standard procedure was adopted of inserting fixed values for L_p and N_p in the solutions for the rudder generated maneuvers and fixed values for L_r and N_r for lateral-control maneuvers. By alternating the execution of the two solutions and successively improving the selection of the fixed values, a consistent set of derivatives could usually be determined in a few iterations.

Maneuvers in which only the rudder or only the control wheel was used to excite the motion also were routinely treated in this way when the maximum-likelihood procedure was used. Sometimes the choice of the values to be fixed could only be made by an interpolation or an extrapolation from results at other test conditions. When the linear-regression solution was used, and if the maneuver was produced solely by a rudder input, the same process of fixing two derivatives (L_p and N_p) was necessary; but in most instances when maneuvers were generated by a control-wheel input, the calculations yielded satisfactory results without fixing any of these four derivative values. These data are indicated in figures 7-9 by open symbols without flags; the data for solutions requiring fixed values are identified by the flagged symbols. From

[1]Reference 14 presents the results of applying a linear-regression computation to obtain longitudinal stability derivatives for the airplane that is the subject of this report. These results are compared with results from a quasi-linearization (modified Newton-Raphson) method, which, like maximum likelihood, is an iterative, "output-error" procedure, with state estimation. This reference notes that the regression method provided smaller standard deviations in the estimated parameter values and better agreement with wind-tunnel measurements than did the quasi-linearization method.

the preceding comments it is seen that when the maximum-likelihood solution was used, for some test conditions it was necessary to have available flight records from a greater number of maneuvers (i.e., additional rudder-excited maneuvers) in order to obtain a satisfactory set of rotary and sideslip derivatives than would be required by the linear-regression solution.

A significant fraction of the maneuvers for which maximum-likelihood solutions were obtained produced results which showed evidence of "nonrandom" deviations of another type.[2] These occur when an error in one of the roll-rate derivatives (C_{ℓ_p}, C_{n_p}, or C_{y_p}) is related to an error in the corresponding lateral-control derivative (C_{ℓ_w}, C_{n_w}, or C_{y_w}). The size of this type of error was observed to be adversely influenced by the following factors associated with the test conditions: (1) a high level of engine thrust at low airspeed, so that the thrust coefficient and C_J were large; (2) a setting of the engine thrust nozzles at angles in the range of 80° to 90°; and (3) a diminished angular range through which the lateral-control surfaces were moved. With regard to the last of these, there were significant deviations in the estimates from a majority of the solutions for flight data in which the maximum displacement of the control wheel was less than 25°.

An example of such errors is observed when, in the same solution, both the calculated value for the lateral-control effectiveness C_{ℓ_w} and the calculated value for roll damping are too large. When solutions showed evidence of such errors, the calculations were repeated with fixed values for the lateral-control derivatives. Because the flight experiments covered an extensive range of test conditions and because most of the solutions were not subject to these errors, there was generally sufficient information to permit the selection of suitable values for the lateral-control derivatives.

Results of applying the maximum-likelihood solution to the data from the maneuvers produced wholly or in part by a lateral-control input when the thrust nozzles were set (nominally) at 85°, are plotted in figures 14(a) and 14(b). On the left in each figure are results from solutions in which the three lateral-control derivatives, C_{ℓ_w}, C_{n_w}, and C_{y_w}, were among the set of estimated parameters. On the right, results from the same test data are plotted but with the values for one or both of the two control derivatives, C_{ℓ_w} and C_{n_w}, fixed, if in the earlier solution they differed substantially from the mean of the results from the other tests. The flagged symbols in these figures identify the lateral-control derivatives that were set at fixed values.[3] The amount of scatter in the graphs of C_{ℓ_p} and C_{n_p} was significantly reduced by inserting the fixed quantities.

Reference 18 presents and discusses other examples illustrating correlation of input and response parameters. In those examples, the correlation is a result of the relationship of elevator displacement and the pitch rate. As in the case of the present investigation, results obtained using a maximum-likelihood algorithm in the

---

[2]Use of the linear-regression solution did not eliminate deviations of this type, but it did reduce the number of instances in which they appeared and decreased the magnitude of the deviations.

[3]In figure 14, solid symbols represent maneuvers that included rudder inputs; open symbols indicate maneuvers made with control-wheel inputs. The latter solutions were obtained with L_r and N_r set at fixed values, selected using the derivative values shown in figures 9(a) and 9(b) as a guide.

examples of reference 18 exhibit larger deviations attributable to this type of correlation than those obtained with linear regression.

CONCLUDING REMARKS

A linear-regression parameter-estimation procedure was used with data from flight experiments to obtain lateral-directional stability and control derivatives for the Augmented Jet Flap Research Aircraft. The tests, which were conducted with the jet flaps deflected to a position typical of a landing approach (65°), covered a large range of angles of attack below the stall, as well as a range of engine power levels up to the rated maximum for continuous operation. The aircraft design enables the pilot to control the direction of the engine propulsive thrust by moving the jet-exhaust nozzles through an angular range of over 90°. The tests included a study of the effects on the derivatives of setting the nozzles — in addition to their positions for forward thrust — at a downward angle that was approximately normal to the aircraft longitudinal axis, and at an intermediate angle that was 60° from the axis. In general, variations in the angle at which the nozzles were set and in the flap jet-momentum coefficient had a rather small effect on the levels of the stability-derivative estimates.

The yaw damping (C_{n_r}) and the derivative C_{ℓ_r} from the flight experiments are generally in agreement with predictions that had been made before the flight program. The flight results also indicate that there was significantly more roll damping at all angles of attack than had been predicted, and that at small angles of attack the effect on roll damping of varying the angle of attack was greater than predicted. The derivative C_{n_p} also shows a variation with angle of attack that is somewhat greater than predicted. Values for the directional derivative C_{n_β} are in agreement with the predicted levels at moderate angles of attack, but they display a sizable decrease with angle of attack that was not predicted.

The results obtained using a maximum-likelihood parameter-estimation procedure are compared with results from the linear-regression calculations. For test conditions corresponding to large values of the flap jet-momentum coefficient (C_J), reduced airspeeds, and to a setting of the engine vectored-thrust nozzles at large angular positions (between 80° and 90°), the maximum-likelihood solutions produced significantly greater dispersion in the estimated-parameter values than did the linear regression. The comparison also indicated that if the linear-regression estimates are biased, as a result of the effects of measurement noise, for these tests the amount of such bias is not large.

Ames Research Center
National Aeronautics and Space Administration
Moffett Field, California 94035, August 24, 1982

APPENDIX A

SIDESLIP VANE ANGLE CORRECTIONS

The sideslip angles indicated by a vane on the nose boom were corrected for sidewash at the vane, using the following relations and assuming that the error varies linearly with the sine of the sideslip angle. Defining β_i as the indicated sideslip angle transferred to the airplane center of gravity and β_c as the actual sideslip angle, a correction factor K_v is defined as

$$K_v = \sin \beta_c / \sin \beta_i \tag{A1}$$

If K_v is known, a corrected side velocity v_c can be obtained with the relation

$$v_c = K_v V \sin \beta_i$$

The longitudinal and vertical components of the true airspeed V, in the body-axis system (at angle of attack α) are, respectively,

$$u = V \cos \beta_c \cos \alpha$$

and

$$w = V \cos \beta_c \sin \alpha$$

The rate of change of side velocity is given by the equation

$$dv_c/dt = A_y - ur + wp + g \cos \theta \sin \phi \tag{A2}$$

The terms A_y, r, p, g, θ, and ϕ are defined in the symbol list. Values of K_v for various flight conditions were determined by performing least-squares fits of the rates of change of the side velocities computed from the vane measurements to the time-histories of dv_c/dt calculated from equation (A2).

APPENDIX B

ROTARY-DERIVATIVE PREDICTIONS

This appendix outlines work by J. Farbridge (of de Havilland of Canada) to modify and extend the results of reference 8, which gives expressions for calculating the lateral-directional rotary-stability derivatives for wings with jet flaps. The derivations in reference 8 include the assumptions that the chord of the flap is small (approaching zero) and that the flap deflection angle is small. Farbridge incorporates the results of reference 19 to account for the effect on the derivatives of a larger flap chord and uses results from reference 20 to estimate the added effect of a large flap deflection. In reference 20 the effect of the flap angle on the lift coefficient of an airfoil section without flap blowing is calculated from theory. By analyzing and correlating experimental lift data on wings with jet flaps, Farbridge deduced the following relation for the lift coefficient of an airfoil due to jet flap blowing:

$$C_{L_{\infty_J}} = 3.5(\alpha_w + \delta_f) - 1.08(\alpha_w + R_c^{0.25}\delta_f)C_J^{0.75} \tag{B1}$$

where R_c is the ratio of flap chord to wing chord and α_w is the wing angle of attack. The total section lift coefficient C_{L_∞} is defined as the sum of $C_{L_{\infty_J}}$ and $C_{L_{\infty_O}}$, the lift on a wing without blowing. The lift coefficient for a finite span wing of aspect ratio A is defined by the following relation:

$$C_{L_A} = (\pi A + 2C_J)C_L/B \tag{B2}$$

where

$$B = \pi A + \partial C_{L_\infty}/\partial\alpha + [C_J/(\delta_f + \alpha_w)]\partial C_{L_\infty}/\partial C_J \tag{B2}$$

The following expressions illustrate the changes in the equation for roll damping that result from Farbridge's modifications. From reference 8,

$$C_{\ell_p} = -\frac{1}{2}\left(\frac{\pi A}{4} + \frac{4}{3}C_J\right)\frac{\partial C_{L_\infty}}{\partial\alpha}\left[\pi A + 2\frac{\partial C_{L_\infty}}{\partial\alpha} + 2C_J\frac{\partial}{\partial C_J}\left(\frac{\partial C_{L_\infty}}{\partial\delta_f}\right)\right]^{-1} \tag{B3}$$

In this equation, C_{L_∞} is replaced by the relation

$$C_{L_\infty} = C_{L_{\infty_J}} + C_{L_{\infty_O}}$$

in which $C_{L_{\infty_J}}$ is from equation (B1), and $C_{L_{\infty_O}}$ is from airfoil-section theory and reference 20. This, with some rearrangement, becomes the following:

$$C_{\ell_p} = -\frac{\pi A}{8}\left[2.42\,C_J^{0.75} + \left(\frac{\partial C_{L_\infty}}{\partial\alpha}\right)_{C_{J=0}}\right]\frac{1 + (16/3)(C_J/\pi A)}{F} \tag{B4}$$

where

$$F = \pi A + 2\left(\frac{\partial C_{L_\infty}}{\partial \alpha}\right)_{C_{J=0}} + C_J^{0.75}\left[4.84 + 5.25\,\frac{(1 - 0.3086\,R_c^{0.25})\delta_f + 0.690\,\alpha + 1.726}{\delta_f + \alpha + 2.5}\right]$$

and

$$\alpha = \alpha_w - 2.5$$

When the expression for C_{n_p} from reference 8 is similarly combined with equation (B1) (and its partial derivatives), the following relation is obtained:

$$C_{n_p} = -\frac{1}{8}\,C_{L_A}\,\frac{\pi A}{\pi A + 2C_J}\left\{1 - 3\left[2.42\,C_J^{0.75} + \left(\frac{\partial C_L}{\partial \alpha}\right)_{C_{J=0}}\right]\frac{1 + (32/9)(C_J/\pi A)}{F}\right\} \tag{B5}$$

where C_{L_A} is the lift coefficient of the wing of the flight vehicle. The expression for C_{ℓ_r} from reference 8 with these modifications is

$$C_{\ell_r} = C_{L_A}\,\frac{\pi A}{8(\pi A + 2C_J)}\left\{\frac{[1 + (16/3)C_J/\pi A]K}{F} + 1\right\} \tag{B6}$$

where

$$K = \left[\pi A + 2.42\,C_J^{0.75} + \left(\frac{\partial C_{L_\infty}}{\partial \alpha}\right)_{C_{J=0}} + \frac{57.3\,C_{L_\infty}}{2(\delta_f + \alpha + 2.5)}\right](1 - H) + I$$

$$H = 5.25\,C_J^{0.75}\,\frac{(1 - 0.3086\,R_c^{0.25})\delta_f + 2.416\,\alpha + 6.04}{C_{L_\infty}}$$

$$I = 3.624\,C_J^{0.75} + \frac{HC_{L_\infty} + 0.405\,C_J^{0.75}[(R_c^{0.25} - 3.241)\delta_f - 2.237\,\alpha - 5.592]}{\delta_f + \alpha + 2.5}$$

The contribution of the wing to the damping in yaw C_{n_r}, as indicated in reference 8, is computed from wing-section drag and is separated into two parts: one due to profile drag $C_{n_{r_o}}$ and one due to induced drag $C_{n_{r_i}}$. As in reference 8, $C_{n_{r_o}} = -(1/4)C_{D_o}$, where C_{D_o} is the profile-drag coefficient. The modified expression for the contribution due to induced drag is

$$C_{n_{r_i}} = -\frac{3}{8}\,C_{L_A}^2\,\frac{\pi A(1 + 32\,C_J/9\pi A)}{(\pi A + 2C_J)^2}\,\frac{K}{F} \tag{B7}$$

The derivatives given by the above equations are referred to stability axes.

APPENDIX C

STABILITY DERIVATIVES USED IN THE SIMULATION MODEL

The following formulas for lateral-directional stability derivatives are from reference 9. They are part of a computer program for the dynamic simulation of the Augmented Jet Research Aircraft. In these expressions, the derivatives are referenced to stability axes, whereas those in the figures (the "predicted" derivatives), like the experimental data, are in the body-axis system. As given here, they apply only for a 65° deflection of the landing flaps. The angle of attack in the formulas is measured from the aircraft fuselage reference and is expressed in degrees.

$$C_{y_\beta} = -1.166 - 0.0344\,\alpha$$

$$C_{y_{\dot\beta}} = -0.0157(\sin\alpha + 4.037\cos\alpha) \qquad \text{(C1)}$$

$$C_{y_r} = 0.1828(\sin\alpha + 4.037\cos\alpha) - 0.0112\,C_{L_A}^2$$

$$C_{y_p} = 0.216\,C_{\ell_p} - 0.15\,C_{L_A} - 0.1828(\cos\alpha - 4.037\sin\alpha) + 0.186$$

$$C_{n_\beta} = 0.000766\,\alpha - 0.0331\,C_J + 0.251$$

$$C_{n_{\dot\beta}} = 0.00193(\sin\alpha + 4.037\cos\alpha)^2 \qquad \text{(C2)}$$

$$C_{n_r} = 0.0735 - 0.0119\,C_{L_A}^2(1 - 0.649\,C_J^{1/2})(1 + 0.00275\,\alpha) - 0.0225(\sin\alpha + 4.037\cos\alpha)^2 - 0.0584\,C_J$$

$$C_{n_p} = -0.00578 - C_{L_A}[0.0860 + 0.00053\,\alpha - 0.02\,C_J] + 0.0225(\sin\alpha + 4.037\cos\alpha)(\cos\alpha - 4.037\sin\alpha - 1.021)$$

$$C_{\ell_\beta} = 0 \text{ (from tests of wind tunnel model with no dihedral)}$$

$$C_{\ell_{\dot\beta}} = -0.00193(\sin\alpha + 4.037\cos\alpha)(\cos\alpha - 4.037\sin\alpha) \qquad \text{(C3)}$$

$$C_{\ell_r} = 0.239\,C_{L_A}(1 - 0.285\,C_J^{1/2})(1 + 0.00231\,\alpha) + 0.0225(\sin\alpha + 4.037\cos\alpha)(\cos\alpha - 4.037\sin\alpha) + 0.045$$

$$C_{\ell_p} = 0.00440\,\alpha - 0.19\,C_J - 0.405$$

APPENDIX D

MATHEMATICAL MODEL AND PARAMETER-ESTIMATION EQUATIONS

This appendix presents the relations and assumptions used to obtain equation (8) and describes the parameter-estimation procedure used in calculating the stability-derivative estimates in this report.

Derivation of the State Equations

The summation terms in equations (5)-(7) represent the linearized aerodynamic force and moment derivatives, as follows.

$$\sum \mathscr{Y}_{\xi_i} \xi_i = \mathscr{Y}_v v + \mathscr{Y}_{\dot{v}} \dot{v} + \mathscr{Y}_r r + \mathscr{Y}_p p + \mathscr{Y}_{\delta_{wa}} \delta_{wa} + \mathscr{Y}_{\delta_{wb}} \delta_{wb} + \mathscr{Y}_{\dot{\delta}} \dot{\delta} + \mathscr{Y}_{\delta_R} \delta_R \tag{D1}$$

$$\sum \mathscr{N}_{\xi_i} \xi_i = \mathscr{N}_v v + \mathscr{N}_{\dot{v}} \dot{v} + \mathscr{N}_r r + \mathscr{N}_p p + \mathscr{N}_{\delta_{wa}} \delta_{wa} + \mathscr{N}_{\delta_{wb}} \delta_{wb} + \mathscr{N}_{\dot{\delta}} \dot{\delta} + \mathscr{N}_{\delta_R} \delta_R \tag{D2}$$

$$\sum \mathscr{L}_{\xi_i} \xi_i = \mathscr{L}_v v + \mathscr{L}_{\dot{v}} \dot{v} + \mathscr{L}_r r + \mathscr{L}_p p + \mathscr{L}_{\delta_{wa}} \delta_{wa} + \mathscr{L}_{\delta_{wb}} \delta_{wb} + \mathscr{L}_{\dot{\delta}} \dot{\delta} + \mathscr{L}_{\delta_R} \delta_R \tag{D3}$$

With the following definitions

$$\begin{aligned} A &= I_{xz}/I_z \\ B &= I_{xz}/I_x \\ C &= 1 - I_{xz}^2/(I_x I_z) \end{aligned} \tag{D4}$$

eliminating $\dot{p}$ and $\dot{r}$, respectively, from equations (2) and (3) yields the expressions:

$$\begin{aligned} \dot{r}C &= v(\mathscr{N}_v + A\mathscr{L}_v) + \dot{v}(\mathscr{N}_{\dot{v}} + A\mathscr{L}_{\dot{v}}) + r(\mathscr{N}_r + A\mathscr{L}_r) + p(\mathscr{N}_p + A\mathscr{L}_p) + \sum_{i=1}^{4} \delta_i(\mathscr{N}_i + A\mathscr{L}_i) \\ \dot{p}C &= v(\mathscr{L}_v + B\mathscr{N}_v) + \dot{v}(\mathscr{L}_{\dot{v}} + B\mathscr{N}_{\dot{v}}) + r(\mathscr{L}_r + B\mathscr{N}_r) + p(\mathscr{L}_p + B\mathscr{N}_p) + \sum_{i=1}^{4} \delta_i(\mathscr{L}_i + B\mathscr{N}_i) \end{aligned} \tag{D5}$$

where δ_i denotes the control variables, δ_{wa}, δ_{wb}, $\dot{\delta}$, and δ_R. From equation (1), and defining $D = 1 - \mathscr{Y}_{\dot{v}}$

$$\dot{v} = \left[\mathscr{Y}_v v + (\mathscr{Y}_v - u)r + (\mathscr{Y}_p + w)p + g \cos\theta \sin\phi + \sum_{i=1}^{4} \mathscr{Y}_{\delta_i} \delta_i \right] \Big/ D \tag{D6}$$

Then with the substitutions

$$N'_\xi = (\mathscr{N}_\xi + A\mathscr{L}_\xi)/C$$

and

$$L'_\xi = (\mathscr{L}_\xi + B\mathscr{N}_\xi)/C \tag{D7}$$

and $\dot{v}$ from equation (D6), equation set (D5) can be written as

$$\dot{r} = v(N'_v + N'_{\dot{v}}\mathscr{Y}_v/D) + r[N'_r + N'_{\dot{v}}(\mathscr{Y}_r - u)/D] + p[N'_p + N'_{\dot{v}}(\mathscr{Y}_p + w)/D]$$

$$+ \sum_{i=1}^{4} \delta_i(N'_{\delta_i} + N'_{\dot{v}}\mathscr{Y}_{\delta_i}/D) + (N'_{\dot{v}}g \cos\theta \sin\phi)/D \tag{D8}$$

$$\dot{p} = v(L'_v + L'_{\dot{v}}\mathscr{Y}_v/D) + r[L'_r + L'_{\dot{v}}(\mathscr{Y}_r - u)/D] + p[L'_p + L'_{\dot{v}}(\mathscr{Y}_p + w)/D]$$

$$+ \sum_{i=1}^{4} \delta_i(L'_{\delta_i} + L'_{\dot{v}}\mathscr{Y}_{\delta_i}/D) + (L'_{\dot{v}}g \cos\theta \sin\phi)/D \tag{D9}$$

Because roll angles during the tests remained relatively small, for this analysis it can be assumed that $\sin\phi = \phi$ and that $\dot{\phi} = p + r\tan\theta_a$, where an average (constant) value, θ_a, is used in place of the varying pitch angle. The state equations can then be written as in equation (8) with the parameters defined by the relations below.

$$Y_v = \mathscr{Y}_v/D \,, \qquad Y_r - u = (\mathscr{Y}_r - u)/D \,,$$
$$Y_p + w = (\mathscr{Y}_p + w)/D \,, \qquad Y_{\delta_i} = \mathscr{Y}_{\delta_i}/D \tag{D10}$$

$$N_v = N'_v + N'_{\dot{v}}\mathscr{Y}_v/D \,, \qquad N_r = N'_r + N'_{\dot{v}}(\mathscr{Y}_r - u)/D \,,$$
$$N_p = N'_p + N'_{\dot{v}}(\mathscr{Y}_p + w)/D \,, \qquad N_{\delta_i} = N'_{\delta_i} + N'_{\dot{v}}\mathscr{Y}_{\delta_i}/D \tag{D11}$$

$$\overline{ND} = (N'_{\dot{v}}g \cos\theta)/D \tag{D12}$$

$$L_v = L'_v + L'_{\dot{v}}\mathscr{Y}_v/D \,, \qquad L_r = L'_r + L'_{\dot{v}}(\mathscr{Y}_r - u)/D \,,$$
$$L_p = L'_p + L'_{\dot{v}}(\mathscr{Y}_p + w)/D \,, \qquad L_{\delta_i} = L'_{\delta_i} + L'_{\dot{v}}\mathscr{Y}_{\delta_i}/D \tag{D13}$$

$$\overline{LD} = (L'_{\dot{v}}g \cos\theta)/D \tag{D14}$$

A value for D based on $C_{y_{\dot{\beta}}}$ given by equation (C1) is estimated in appendix E. For a typical set of test conditions, D is calculated to be 1.002, and it varies only slightly from this at other conditions of the tests.

The following relations were used to compute the stability and control derivatives that are presented in this report. The true velocity V and the dynamic pressure $\bar{q}$ $[=(1/2)\rho V^2]$ are the average values for the time of the maneuver.

$$
\begin{aligned}
C_{y_\beta} &= Y_v VW/\bar{q}Sg) \\
C_{n_\beta} &= (N_v - AL_v)VI_z/(\bar{q}Sb) \\
C_{\ell_\beta} &= (L_v - BN_v)VI_x/(\bar{q}Sb) \\
C_{y_r} &= 2Y_r VW/(\bar{q}Sbg) \\
C_{n_r} &= 2(N_r - AL_r)VI_z/(\bar{q}Sb^2) \\
C_{\ell_r} &= 2(L_r - BN_r)VI_x/(\bar{q}Sb^2) \\
C_{y_p} &= 2Y_p VW/(\bar{q}Sbg) \\
C_{n_p} &= 2(N_p - AL_p)VI_z/(\bar{q}Sb^2) \\
C_{\ell_p} &= 2(L_p - BN_p)VI_x/(\bar{q}Sb^2)
\end{aligned}
\tag{D15}
$$

The control-deflection derivatives are computed from the following equations, where δ represents the variables δ_{wa}, δ_{wb}, $\dot{\delta}$, and δ_R.

$$
\begin{aligned}
C_{y_\delta} &= Y_\delta W/(\bar{q}Sg) \\
C_{n_\delta} &= (N_\delta - AL_\delta)I_z/(\bar{q}Sb) \\
C_{\ell_\delta} &= (L_\delta - BN_\delta)I_x/(\bar{q}Sb)
\end{aligned}
\tag{D16}
$$

The control-wheel derivatives are calculated from the relation $C_{\Lambda_w} = C_{\Lambda_{wa}} + C_{\Lambda_{wb}}$ in which Λ corresponds to the subscripts y, n, and ℓ.

Parameter Estimation

It is assumed that the system is described by the vector differential equation

$$\dot{x}(t) = Fx(t) + Gu(t) + w(t) \; ; \qquad x(t_o) = x_o \tag{D17}$$

where $x(t)$ is a state vector, $u(t)$ is an input vector, $w(t)$ is the state (or process) noise vector, x_o is the initial condition vector, and F and G are, respectively, the stability and control matrices. The system output can be expressed as

$$y^T(t) = [x_m^T(t), \; a_m^T(t)] \tag{D18}$$

where $x_m(t)$ and $a_m(t)$ are state and state-derivative vector elements; the complete state-derivative vector can be expressed as

$$a(t) = F_a x(t) + Gu(t) + w(t) \tag{D19}$$

where F_a is a subset of F. The parameter-estimation procedure outlined here (excerpted from ref. 16) is formulated to allow the selection of a maximum-likelihood or a linear-regression solution to estimate the unknown parameters in the stability and control matrices. The data system yields a time-history record on an interval (t_o,t_f) with samples spaced T seconds apart comprising control inputs $u(t)$ and the record

$$z(t_i) = y(t_i) + v(t_i) , \quad i = 0, 1, \ldots, N - 1$$

where $z(t_i)$ and $v(t_i)$ are measurement and measurement-noise vectors, respectively. (Other assumptions: that the measurement noise and the process noise $w(t)$ are white-Gaussian with means, respectively, of y_b and w_b.)

In the maximum-likelihood parameter-estimation procedure, a model estimate $\hat{z}(t)$ is matched to a data record $z(t)$ by adjusting model parameters with an iterative strategy to minimize an error criterion. If the flight maneuver is performed under conditions that are relatively free of atmospheric turbulence, the random component of $w(t)$ in equation (D17) can be ignored and a state estimate is obtained from the model

$$\dot{\hat{x}}(t) = F\hat{x}(t) + Gu(t) + w_b ; \quad \hat{x}(t_o) = x_o \tag{D20}$$

where w_b can account for bias error in the measurement of $u(t)$. The model output is given by

$$\hat{y}^T(t) = [\hat{x}_m^T, \hat{a}_m^T(t)]$$

where the state-derivative estimates would be taken as a subset of

$$\hat{a}(t) = F_a\hat{x}(t) + Gu(t) + w_b \tag{D21}$$

Then an estimate of the data record is formed as

$$\hat{z}(t_i) = \hat{y}(t_i) + v_b ; \quad i = 0, 1, \ldots, N - 1 \tag{D22}$$

Here v_b represents a constant bias in the measurement of $y(t)$.

The parameter vector can be written as

$$p^T = p_{FG}^T, p_{w_b}^T, p_{x_o}^T, p_{v_b}^T \tag{D23}$$

For the maximum-likelihood formulation the criterion for matching the model output to the data record is the "cost function":

$$J = (1/2) \sum_{i=0}^{N-1} [z(t_i) - \hat{z}(t_i)]^T B^{-1} [z(t_i) - \hat{z}(t_i)] + (N/2)\log|B| \qquad (D24)$$

where the minimizing value of B is given by

$$B = (1/N) \sum_{i=0}^{N-1} [z(t_i) = \hat{z}(t_i)][z(t_i) - \hat{z}(t_i)]^T \qquad (D25)$$

This criterion is minimized with a modified Newton-Raphson (or quasi-linearization) algorithm (ref. 11). A parameter change is computed as $\delta p = -M^{-1}(\partial J/\partial p)^T$, where M is given by

$$M = \sum_{i=0}^{N-1} S^T(t_i) B^{-1} S(t_i) \qquad (D26)$$

and the gradient vector $\partial J/\partial p$ is

$$(\partial J/\partial p) = -\sum_{i=0}^{N-1} [z(t_i) - \hat{z}(t_i)]^T B^{-1} S(t_i) \qquad (D27)$$

In the above equations, $S(t)$ is the sensitivity matrix

$$S(t) = \partial \hat{z}(t)/\partial p$$

For a linear-regression fit with no process noise,

$$\hat{z}(t) = \hat{a}_m(t)$$

and the kth column of $S(t)$ can be obtained as a subset of the vector

$$[\partial \hat{a}(t)/\partial p_k] = (\partial F_a/\partial p_k)\hat{x}(t) + (\partial G/\partial p_k)u(t) + (\partial w_b/\partial p_k)$$

if, as is the case in the present application, all the states are available among the measurements. For a maximum-likelihood solution, the evaluation of $S(t)$ requires the solution of as many as n_e differential equations during each iteration, where n_e is the product of the number of states and the number of unknown parameters. Thus, in the process-noise-free case, from equation (D22),

$$S(t) = [\partial \hat{y}(t)/\partial p] + (\partial v_b/\partial p) \qquad (D28)$$

which implies that both $\partial \hat{x}_m(t)/\partial p$ and $\partial \hat{a}_m(t)/\partial p$ must be computed. The kth column of the state-sensitivity matrix $\partial \hat{x}(t)/\partial p$ is obtained from equation (D20) as the solution of the vector differential equation

$$[\partial \hat{x}(t)/\partial p_k] = F[\partial \hat{x}(t)/\partial p_k] + (\partial F/\partial p_k)\hat{x}(t) + (\partial G/\partial p_k)u(t) + \partial w_b/\partial p_k \qquad (D29)$$

with initial conditions

$$\partial\hat{x}(0)/\partial p_k = \begin{cases} 0, & p_k \text{ not in } x_o \\ \varepsilon, & p_k \text{ in } x_o \end{cases}$$

Here ε is a vector with zero elements, except for a one in the row corresponding to an initial-condition parameter p_k.

To increase the convergence range of the quasi-linearization algorithm, a procedure known as a "Denery start" (ref. 17) is included in the computational program. In this procedure, equation (D29) is modified by solving the state sensitivity equations, using state measurements in place of $\hat{x}(t)$.

APPENDIX E

COMPUTED EFFECTS OF $\dot{\beta}$ DERIVATIVES ON PARAMETER ESTIMATES

In this appendix the effect on the stability derivatives of sidewash due to sideslip is calculated. The extracted parameter values include contributions from this induced sidewash. These contributions are shown in equations (D10) through (D14) as the terms in which the subscript $\dot{v}$ (or the symbol D or both) appears. In the expressions below, the magnitude of their contribution to the stability and control derivative values is computed, based on the predicted values for $C_{y_{\dot{\beta}}}$, $C_{n_{\dot{\beta}}}$, and $C_{\ell_{\dot{\beta}}}$ that were used in the simulation model and are presented in appendix C. To apply a correction to the extracted derivative values for this effect, the following increments would be subtracted from values shown in this report.

Side force:

$$\Delta C_{y_\lambda} = EC_{y_\lambda} C_{y_{\dot{\beta}}} \tag{E1}$$

where $E = \rho Sbg/(4W)$ and λ denotes the variables β, r, p, δ_w, and δ_R.

Yawing moment:

$$\Delta C_{n_\beta} = EC_{y_\beta} C_{n_{\dot{\beta}}}$$

$$\Delta C_{n_r} = -\left(\cos \alpha - EC_{y_r}\right) C_{n_{\dot{\beta}}}$$

$$\Delta C_{n_p} = \left(\sin \alpha + EC_{y_p}\right) C_{n_{\dot{\beta}}}$$

$$\Delta C_{n_\delta} = EC_{y_\delta} C_{n_{\dot{\beta}}}$$

Rolling moment:

$$\Delta C_{\ell_\beta} = EC_{y_\beta} C_{\ell_{\dot{\beta}}}$$

$$\Delta C_{\ell_r} = -\left(\cos \alpha - EC_{y_r}\right) C_{\ell_{\dot{\beta}}}$$

$$\Delta C_{\ell_p} = \left(\sin \alpha + EC_{y_p}\right) C_{\ell_{\dot{\beta}}}$$

$$\Delta C_{\ell_\delta} = EC_{y_\delta} C_{\ell_{\dot{\beta}}}$$

The side force increments can all be expressed as a fraction of the side-force derivative,

$$\Delta C_{y_\lambda} / C_{y_\lambda} = EC_{y_{\dot{\beta}}} \tag{E2}$$

With $C_{y_{\dot{\beta}}}$ given by equation (C1), this relation indicates a change of less than 0.4% of the derivative values under any conditions of the tests. Also using equation (C1), the value for D in equations (D-6) through (D14) can be computed:

$$\begin{aligned} D &= 1.0 - \mathscr{Y}_{\dot{v}} \\ &= 1.0 - EC_{y_{\dot{\beta}}} \\ &= 1.002 \end{aligned} \tag{E3}$$

for a typical set of test conditions and varies only slightly for other test conditions.

Increments to the yawing- and rolling-moment derivatives from the above formulas are listed below for three angles of attack, 2°, 7°, and 12° (corresponding to, respectively, assumed equivalent airspeeds of 90, 75, and 65 knots), an aircraft gross weight of 178,000 N (40,000 lb) and an altitude of 925 m (3,000 ft).

α	2°	7°	12°
ΔC_{n_β}	-0.0014	-0.0014	-0.0014
ΔC_{ℓ_β}	.0003	.0002	.0000
ΔC_{n_r}	-.0308	-.0299	-.0283
ΔC_{ℓ_r}	.0066	.0038	.0009
ΔC_{n_p}	.0007	.0033	.0061
ΔC_{ℓ_p}	-.0001	-.0004	-.0002
ΔC_{n_w}	.0008	.0005	.0004
ΔC_{ℓ_w}	.0002	.0001	.0000
$\Delta C_{n_{\delta_R}}$	.0000	.0000	.0000
$\Delta C_{\ell_{\delta_R}}$	.0000	.0000	.0000

Except for yaw damping, C_{n_r}, all of these values represent negligibly small corrections to the extracted derivative values. If C_{n_r} is corrected by the amount shown above, the yaw damping would be reduced by between 6% and 9%.

REFERENCES

1. Quigley, Hervey C.; Innis, Robert C.; and Grossmith, Seth: A Flight Investigation of the STOL Characteristics of an Augmented Jet Flap STOL Research Aircraft. NASA TM X-62,334, 1974.

2. Ashleman, R. H.; and Skavdahl, H.: The Development of an Augmentor Wing Jet STOL Research Aircraft (Modified C-8A), Vol. I, Summary. NASA CR-114,504, 1972.

3. Vomaske, Richard F.; Innis, Robert C.; Swan, Brian E.; and Grossmith, Seth W.: A Flight Investigation of the Stability, Control and Handling Qualities of an Augmented Jet Flap STOL Airplane. NASA TP-1254, 1978.

4. Campbell, John P.; and McKinney, Marion O.: Summary of Methods for Calculating Dynamic Lateral Stability and Response and for Estimating Lateral Stability Derivatives. NASA TR-1098, 1952.

5. Finck, R. D.: USAF Stability and Control DATCOM. Second ed., McDonnell Douglas Corp., 1976. (Also USAF Stability and Control DATCOM. Second ed., Air Force Flight Dynamics Laboratory, U.S. Air Force, 1976.)

6. Koenig, David G.; Corsiglia, Victor R.; and Morelli, Joseph P.: Aerodynamic Characteristics of a Large-Scale Model with an Unswept Wing and Augmented Jet Flap. NASA TN D-4610, 1968.

7. Cook, Anthony M.; and Aiken, Thomas N.: Low Speed Aerodynamic Characteristics of a Large Scale STOL Transport Model with an Augmented Jet Flap. NASA TM X-62,017, 1971.

8. Thomas, H. H. B. M.; and Ross, A. J.: The Calculation of the Rotary Lateral Stability Derivatives of a Jet-Flapped Wing. RAE Tech. Note Aero. 2545, 1958.

9. Cleveland, William B.; Vomaske, Richard F.; and Sinclair, S. R. M.: Augmentor Wing Jet STOL Research Aircraft Digital Simulation Model. NASA TM X-62,149, 1972.

10. Klein, Vladislav: Determination of Stavility and Control Parameters of a Light Airplane from Flight Data Using Two Estimation Methods. NASA TP-1306, 1979.

11. Iliff, Kenneth W.; and Taylor, Lawrence W., Jr.: Determination of Stability Derivatives from Flight Data Using a Newton-Raphson Minimization Technique. NASA TN D-6579, 1972.

12. Parrish, Russell V.; and Steinmetz, George G.: Lateral Stability and Control Derivatives of a Jet Fighter Airplane Extracted from Flight Test Data by Utilizing Maximum Likelihood Estimation. NASA TN D-6905, 1972.

13. Klein, Vladislav: Identification Evaluation Methods. Parameter Identification, AGARD Lecture Series No. 104, 1979, p. 2-1.

14. Wingrove, Rodney C.: Parameter Estimation of Powered-Lift STOL Aircraft Characteristics Including Turbulence and Ground Effects. NASA TM X-62,382, 1974.

15. Iliff, Kenneth W.; and Maine, Richard E.: Practical Aspects of Using a Maximum Likelihood Estimation Method to Extract Stability and Control Derivatives from Flight Data. NASA TN D-8209, 1976.

16. Bach, Ralph E., Jr.: A User's Manual for Ames (A Parameter Estimation Program). NASA CR-163118, 1974.

17. Denery, Dallas G.: Identification of System Parameters from Input-Output Data with Application to Air Vehicles. NASA TN D-6468, 1971.

18. Wingrove, R. C.: Estimation of Longitudinal Aircraft Characteristics Using Parameter Identification Techniques. 9th Annual Symposium of the Society of Flight Test Engineers, Arlington, Texas, Oct. 4-6, 1978.

19. Spence, D. A.: The Lift of a Thin Aerofoil with a Jet-Augmented Flap. Aeronaut. Quart., vol. 9, Aug. 1958, pp. 287-299.

20. Hay, J. A.; and Eggington, W. J.: An Exact Theory of a Thin Aerofoil with Large Flap Deflection. J. Roy. Aeronaut. Soc., Nov. 1956, pp. 753-757.

TABLE 1.- AUGMENTED JET FLAP RESEARCH AIRCRAFT: WEIGHTS AND AREAS

Weights, N (lb)	
Maximum gross	213,000 (48,000)
Operational, empty	145,000 (32,600)
Areas, m^2 (ft^2)	
Wing	80.36 (865)
Horizontal tail	21.65 (233)
Vertical tail	14.12 (152)
Other geometric data	
Wing dihedral, starting at station 5.36 m from plane of symmetry, deg	5
Ailerons	
Span, m (ft)	3.51(11.50)
Chord aft of hinge line, m (ft)	.61 (2.01)
Spoilers	
Span, m (ft)	3.44(11.30)
Chord, m (ft)	.36 (1.18)
Position of hinge line, % wing chord, average	62.4
Flaps	
Span (each side), m (ft)	7.01(23.0)
Chord aft of hinge line, m (ft)	.98 (3.2)

Moments of inertia, kg-m^2 (slug-ft^2)
(Gross weight 178,000 N (40,000 lb))
With original elevator control (spring tab):
I_x = 357,000 (263,300)
I_y = 278,000 (205,000)
I_z = 587,000 (432,900)
With modified elevator control (powered elevator)
I_x = 361,000 (266,300)
I_y = 316,000 (233,100)
I_z = 620,000 (457,300)

Product of inertia
I_{xz} = 48,130 (35,500)

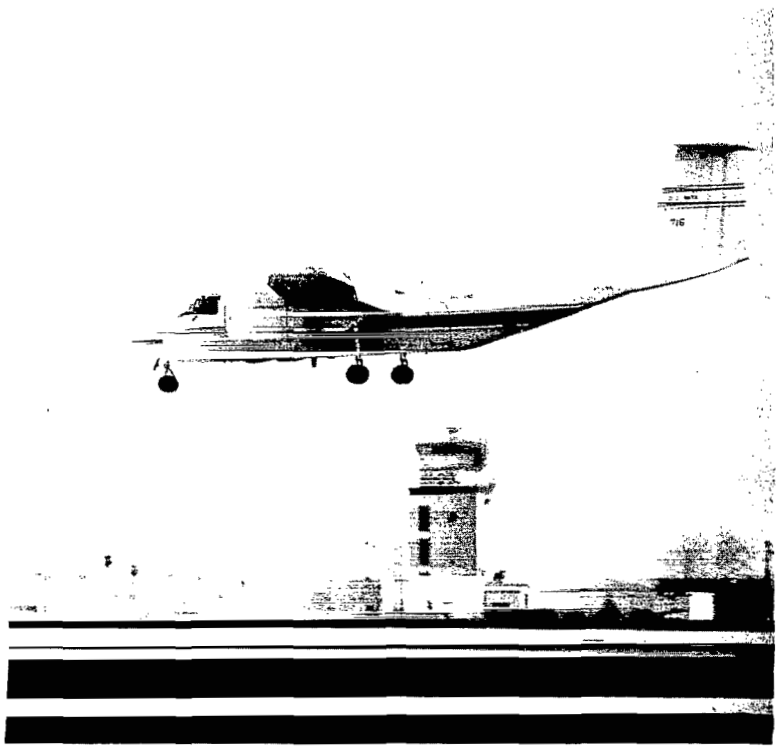

Figure 1.- Augmented Jet Flap Research Aircraft in landing configuration.

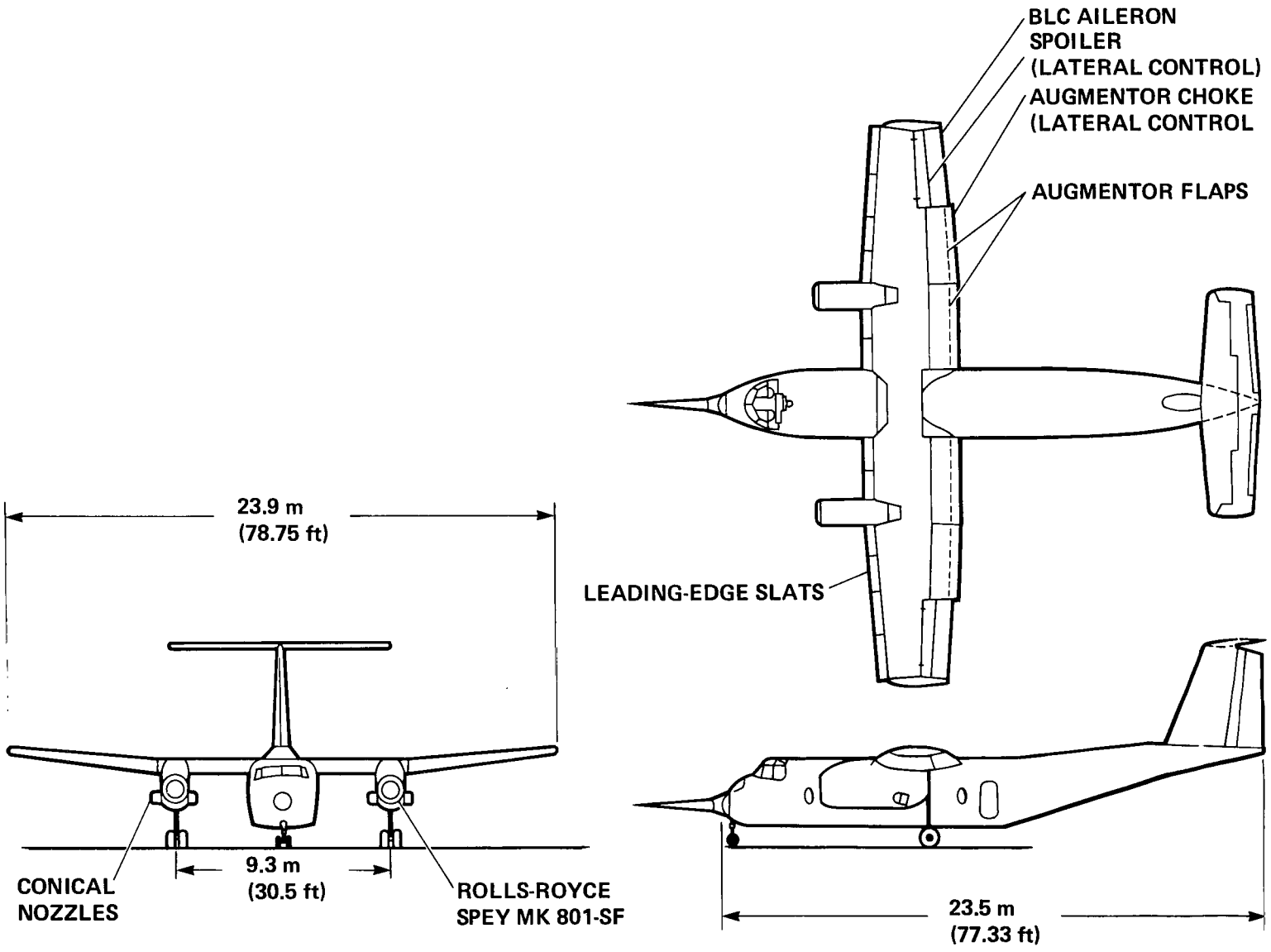

Figure 2.- Three-view drawing of the Augmented Jet Flap Research Aircraft.

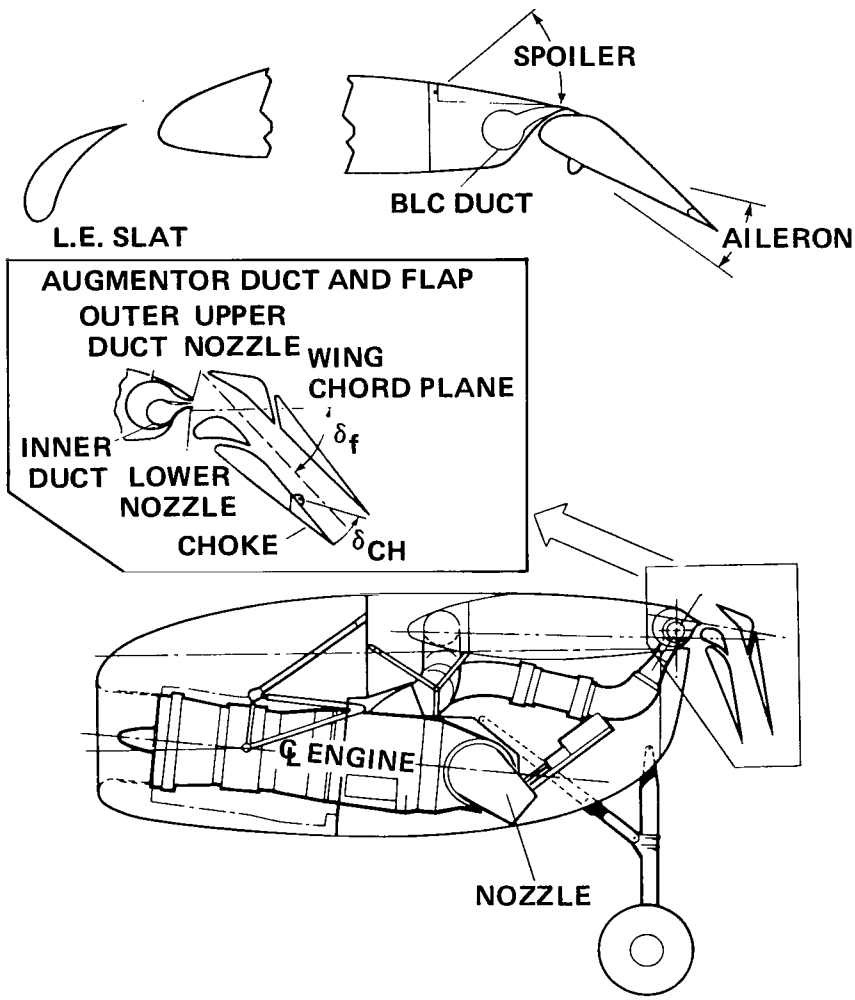

Figure 3.- Details of the engine installation, lateral control surfaces, and augmented jet-flap components.

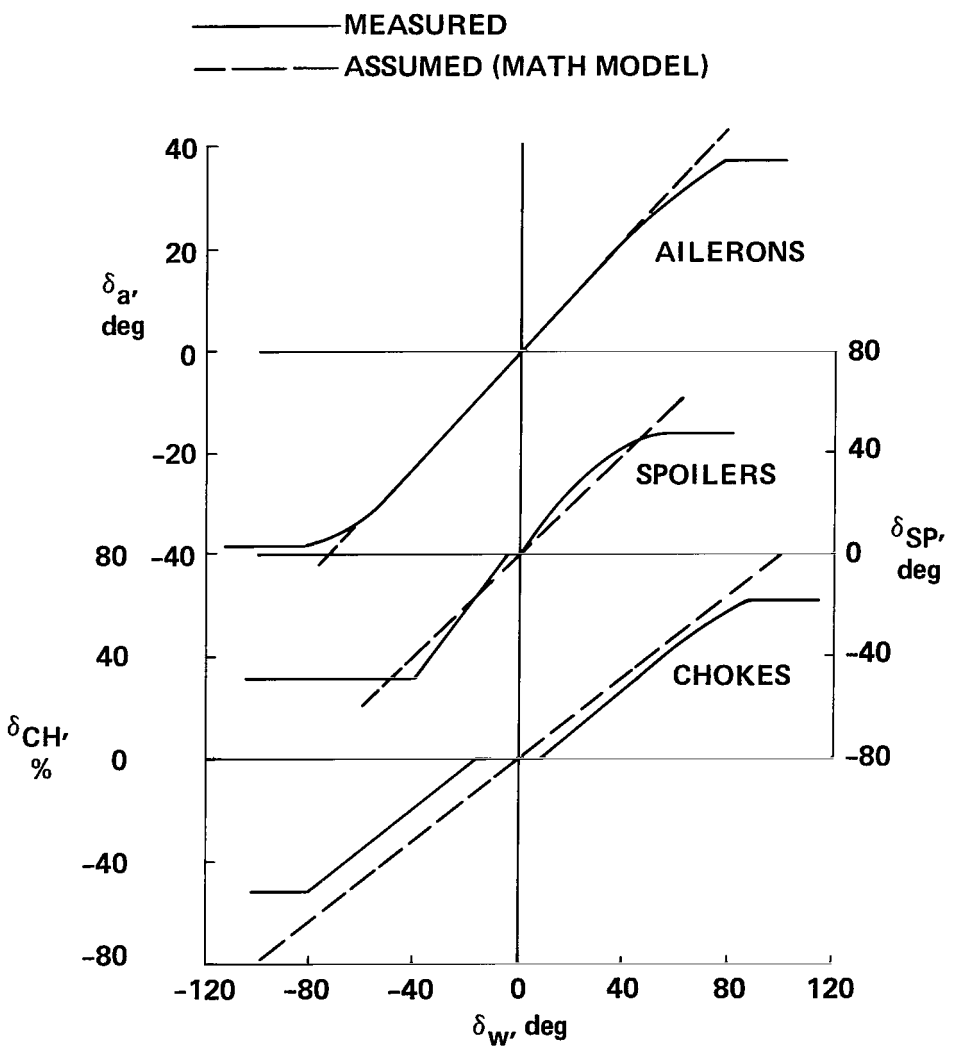

Figure 4.- Deflections of the lateral control surfaces as functions of control-wheel angle.

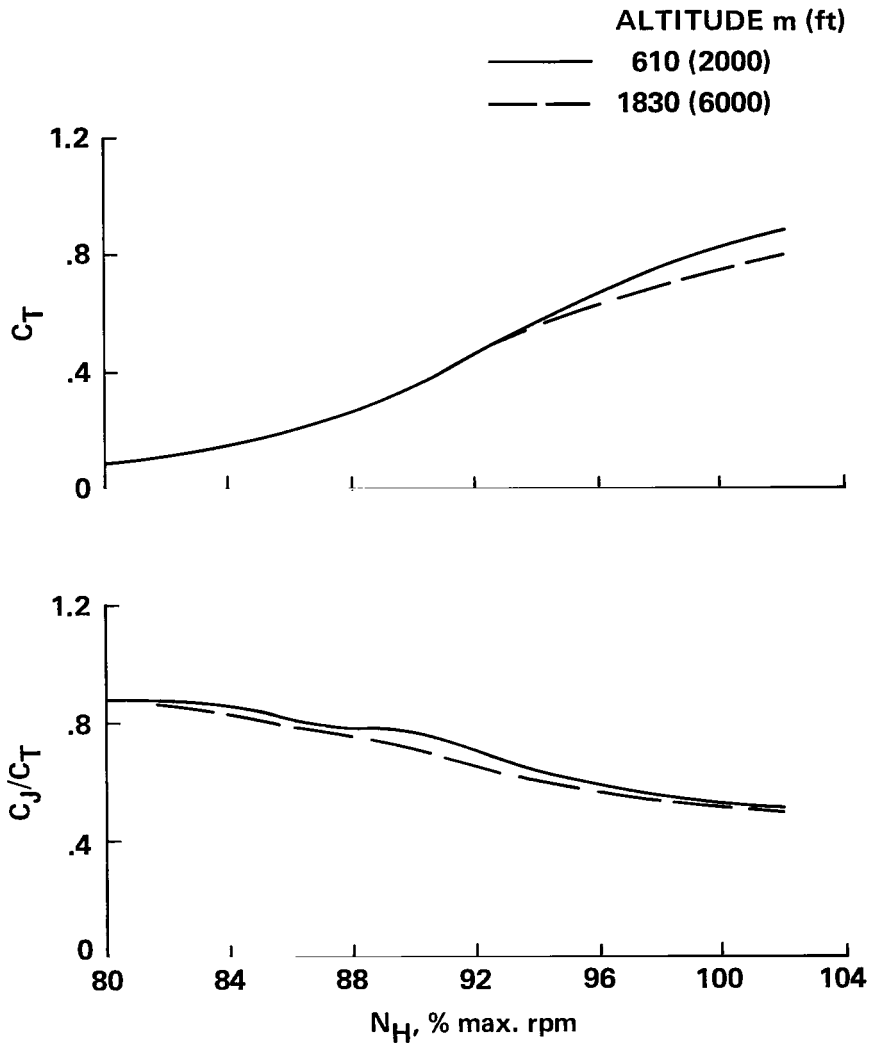

Figure 5.- Engine thrust and jet-flap flow characteristics at two altitudes (equivalent airspeed, 70 knots).

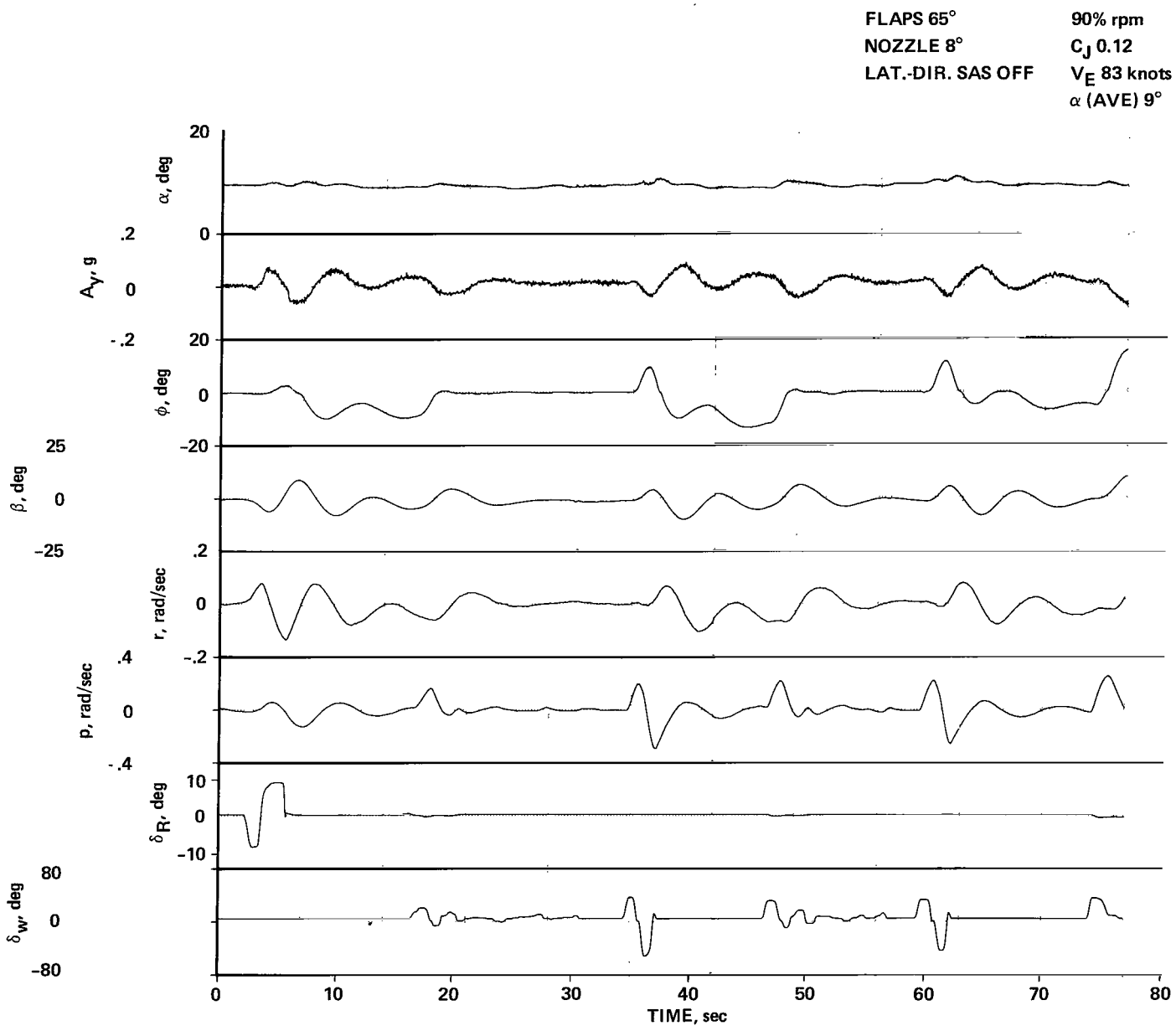

Figure 6.- Typical time-history record of a maneuver resulting from a rudder input followed by a control-wheel input.

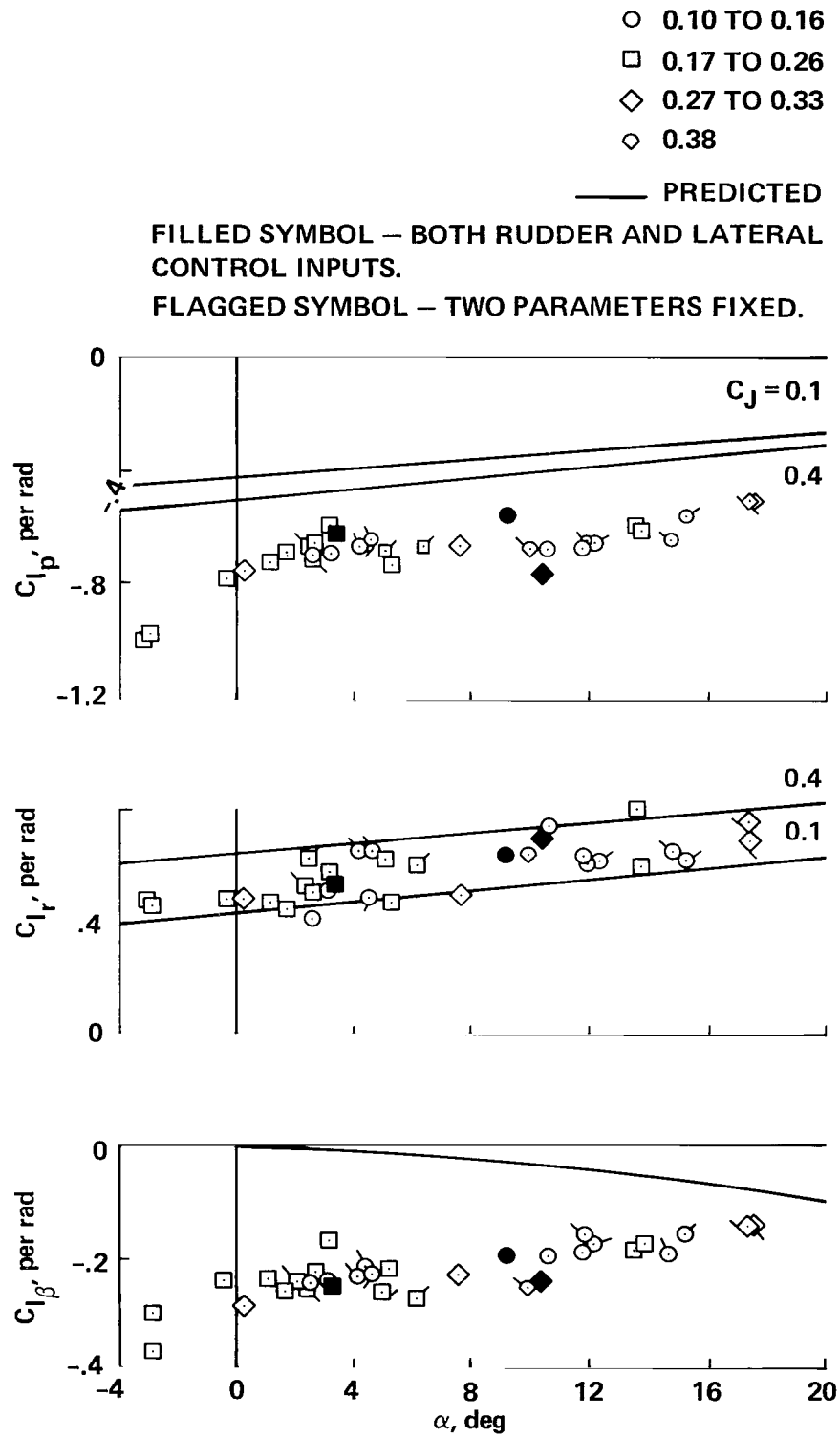

(a) C_{ℓ_p}, C_{ℓ_r} and C_{ℓ_β} vs α.

Figure 7.- Lateral-directional stability derivatives: nozzles at 8°.

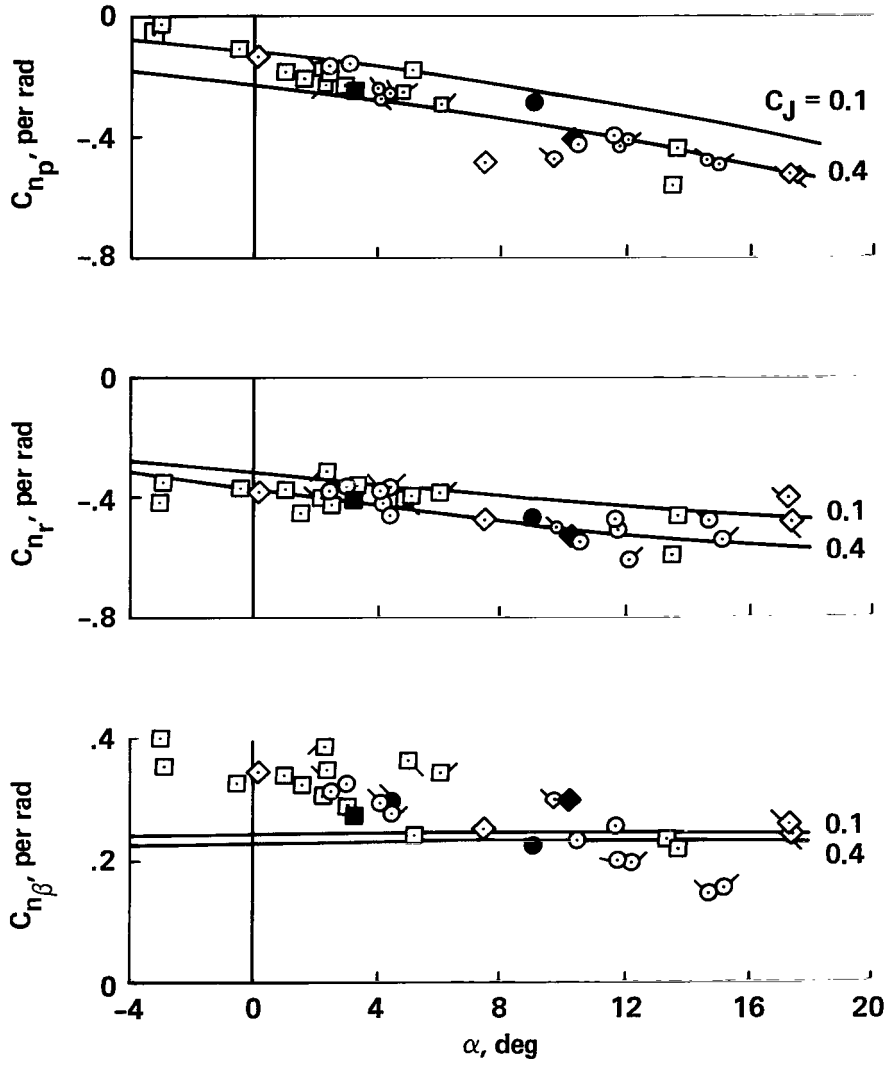

(b) C_{n_p}, C_{n_r} and C_{n_β} vs α.

Figure 7.- Continued.

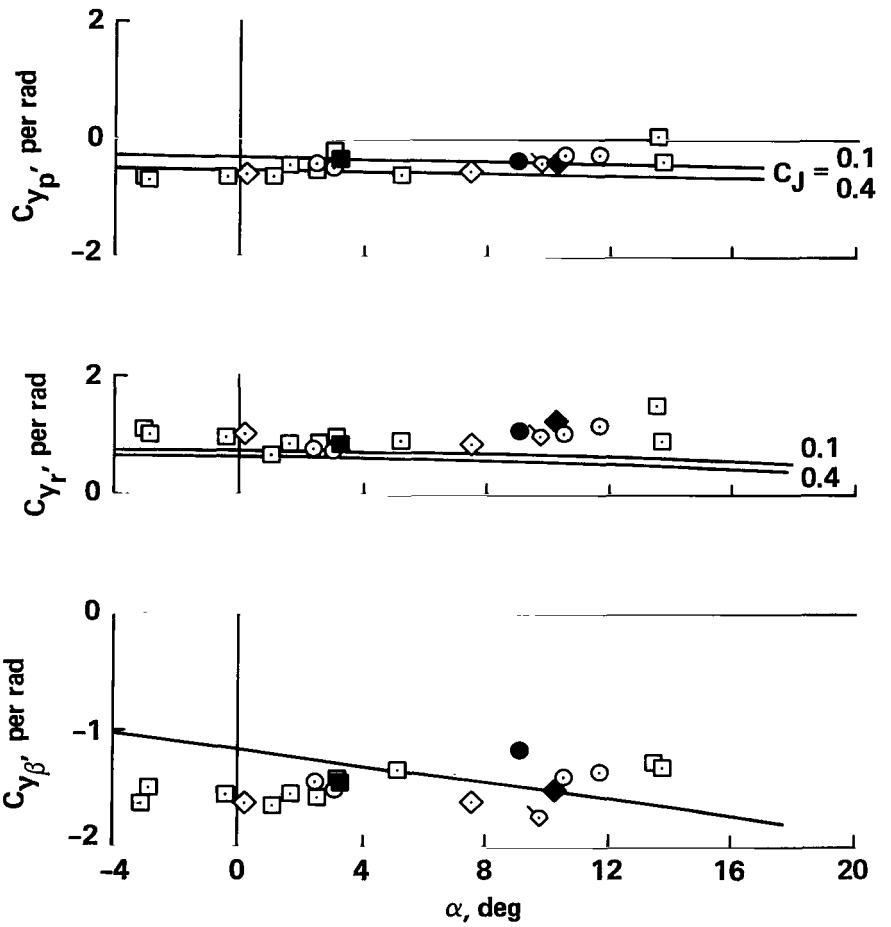

(c) C_{y_p}, C_{y_r}, and C_{y_β} vs α.

Figure 7.- Concluded.

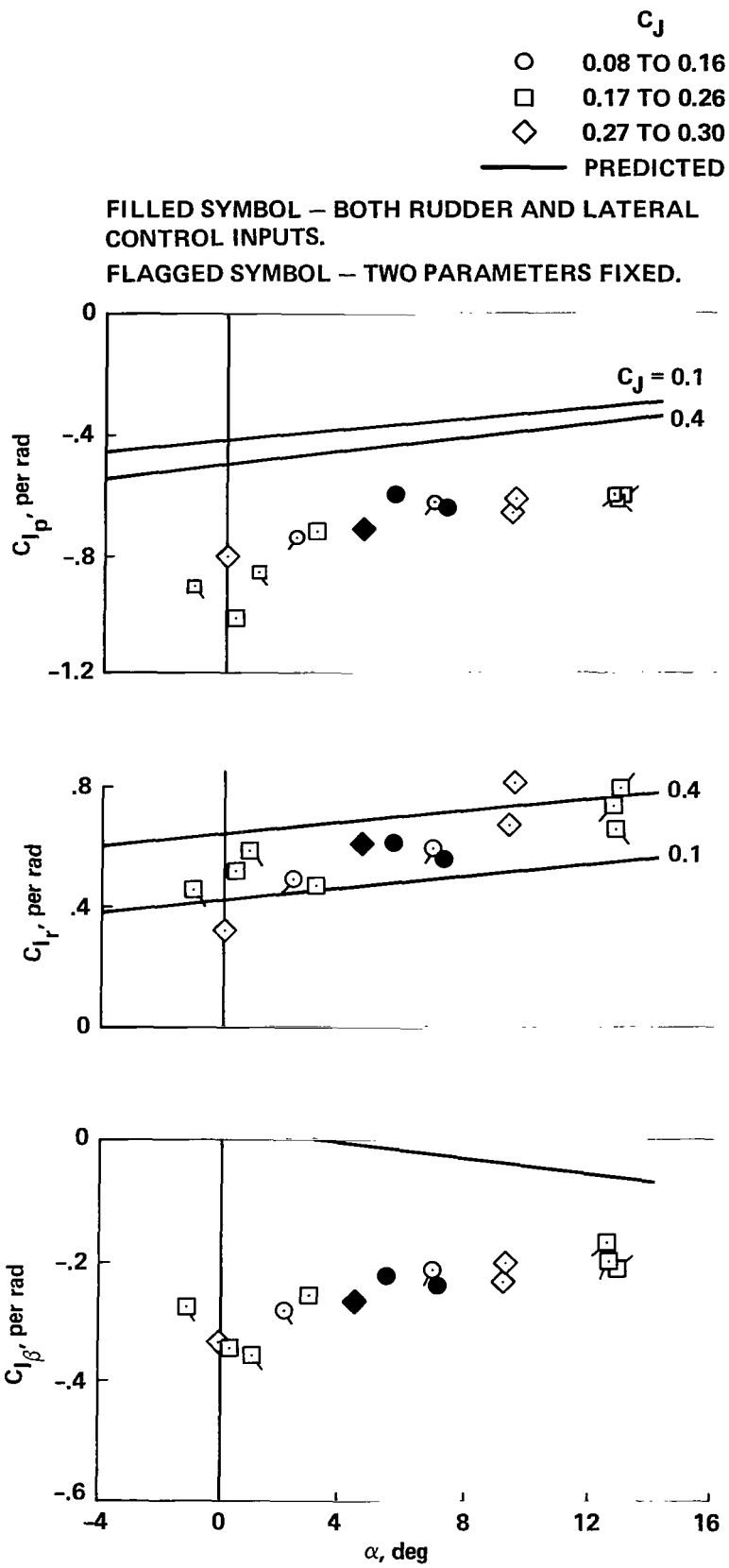

(a) C_{ℓ_p}, C_{ℓ_r}, and C_{ℓ_β} vs α.

Figure 8.- Lateral-directional stability derivatives: nozzles at 60°.

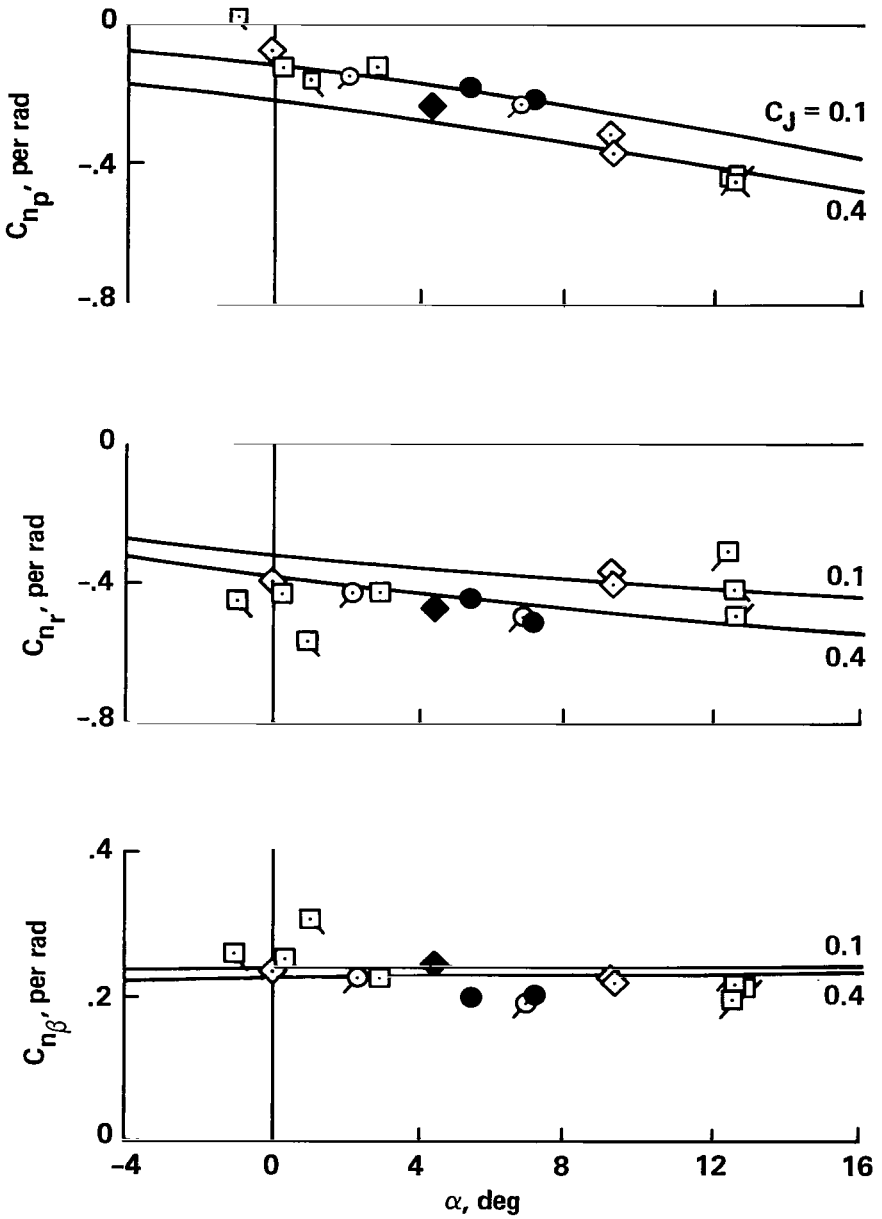

(b) C_{n_p}, C_{n_r}, and C_{n_β} vs α.

Figure 8.- Continued.

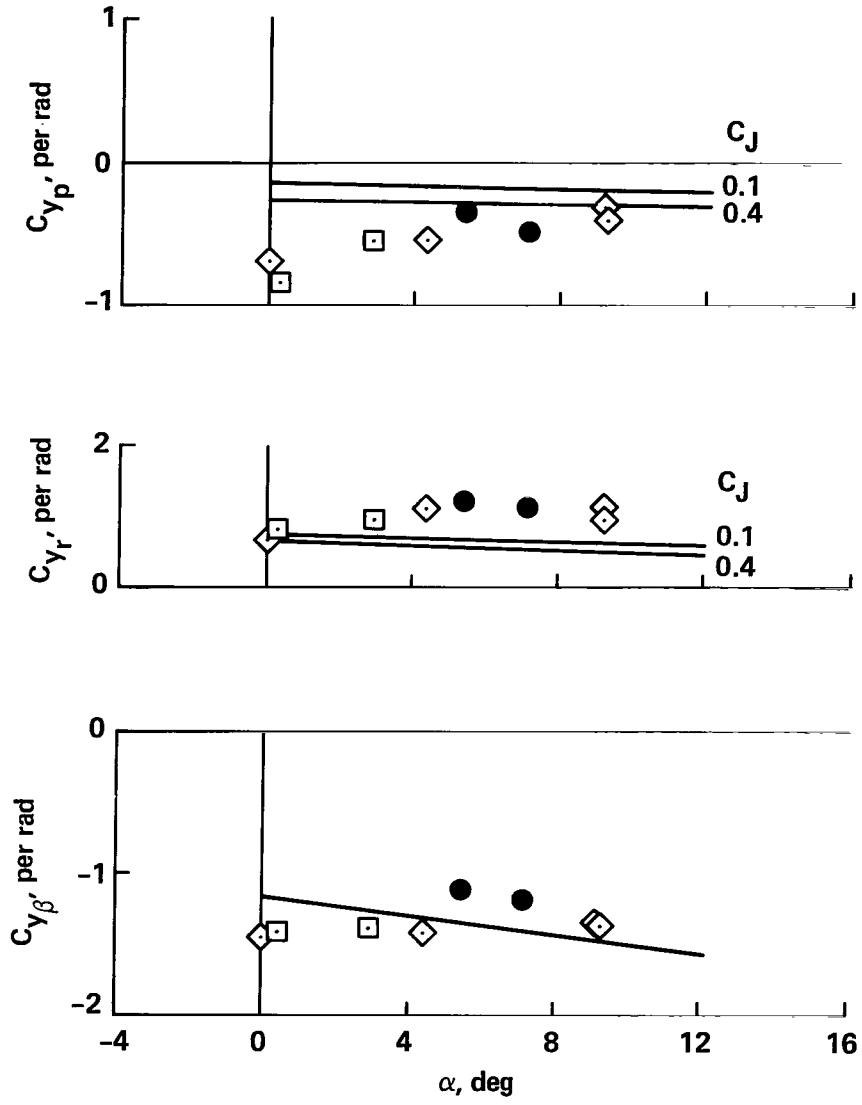

(c) C_{y_p}, C_{y_r}, and C_{y_β} vs α.

Figure 8.- Concluded.

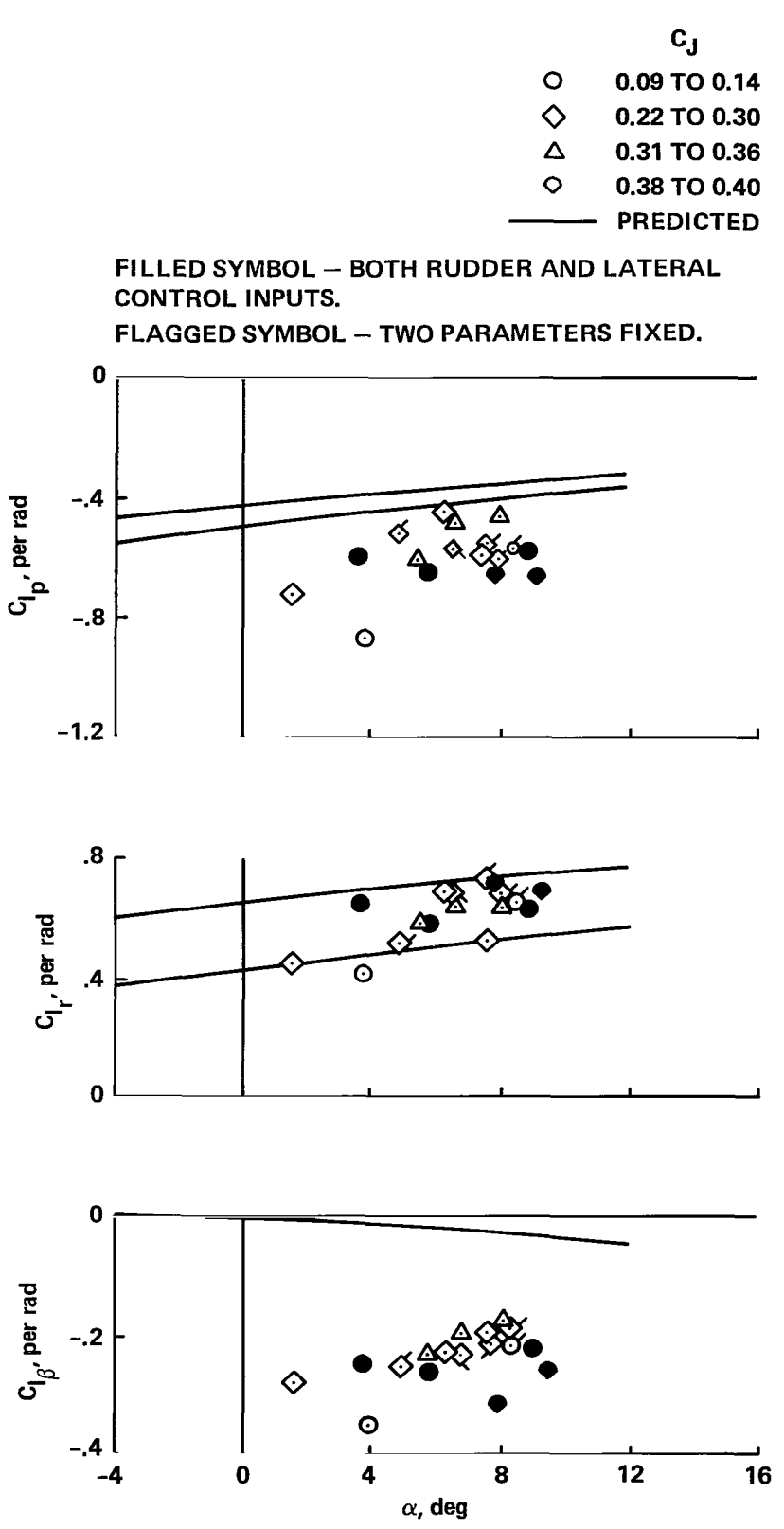

(a) C_{ℓ_p}, C_{ℓ_r}, and C_{ℓ_β} vs α.

Figure 9.- Lateral-directional stability derivatives: nozzles at 80° to 90°.

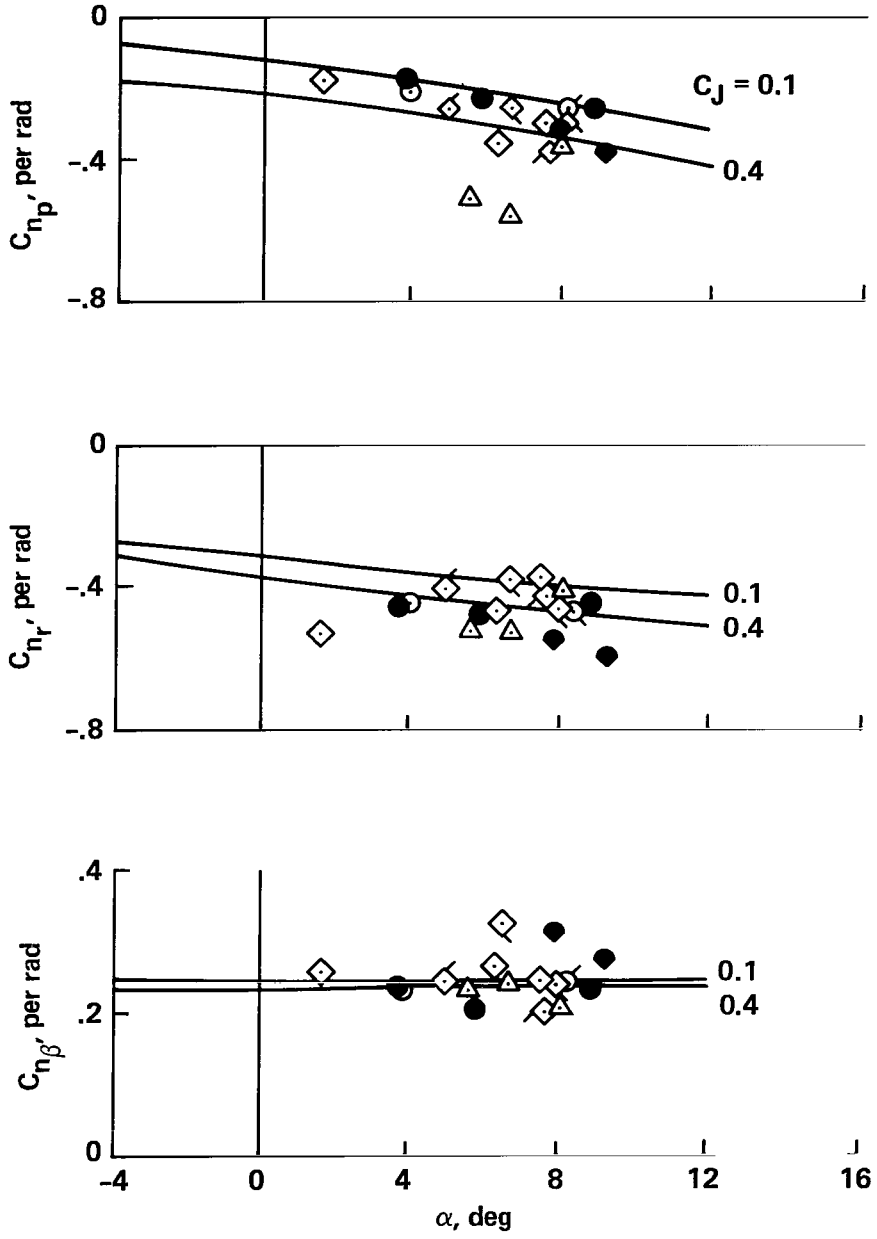

(b) C_{n_p}, C_{n_r}, and C_{n_β} vs α.

Figure 9.- Continued.

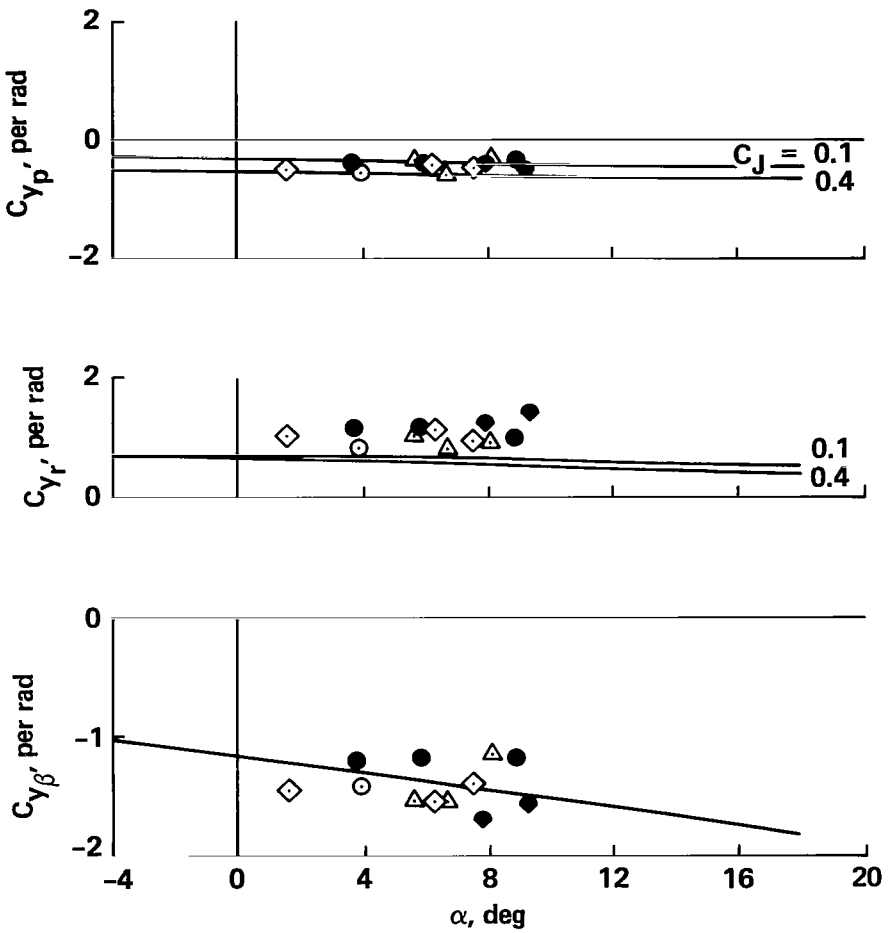

(c) C_{y_p}, C_{y_r}, and C_{y_β} vs α.

Figure 9.- Concluded.

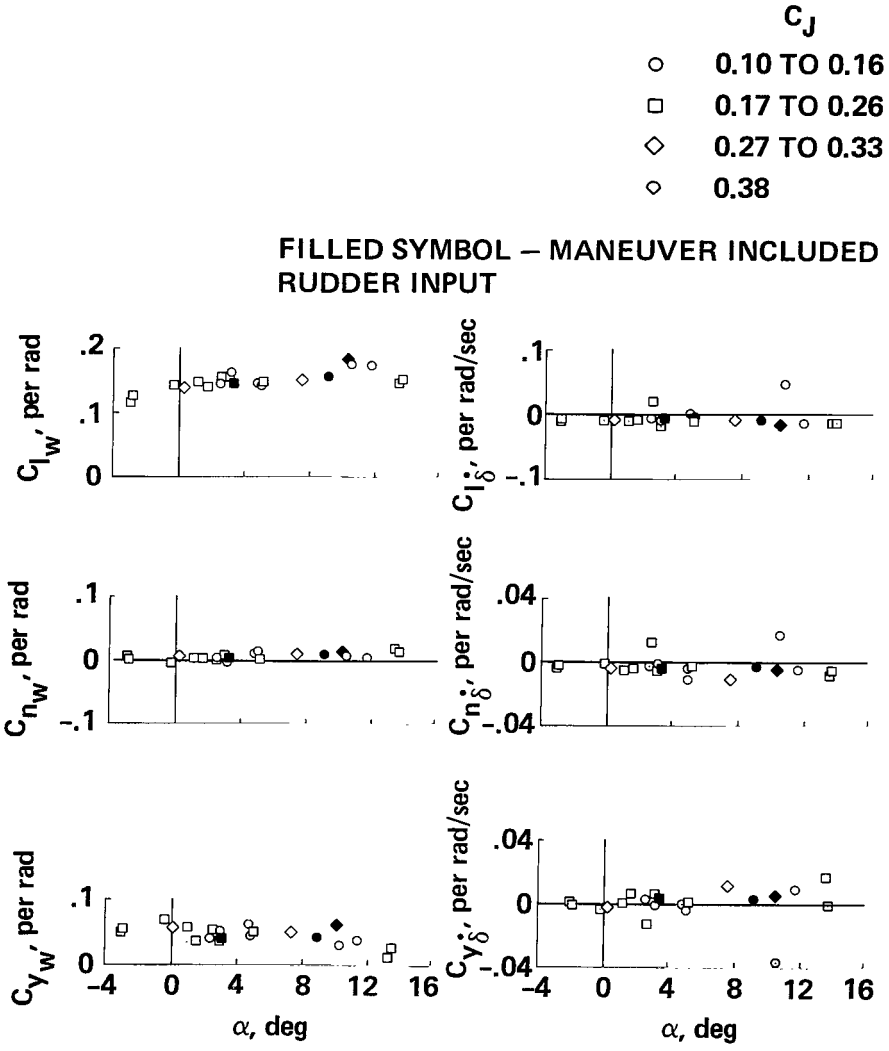

(a) Nozzles at 8°.

Figure 10.- Lateral-control characteristics.

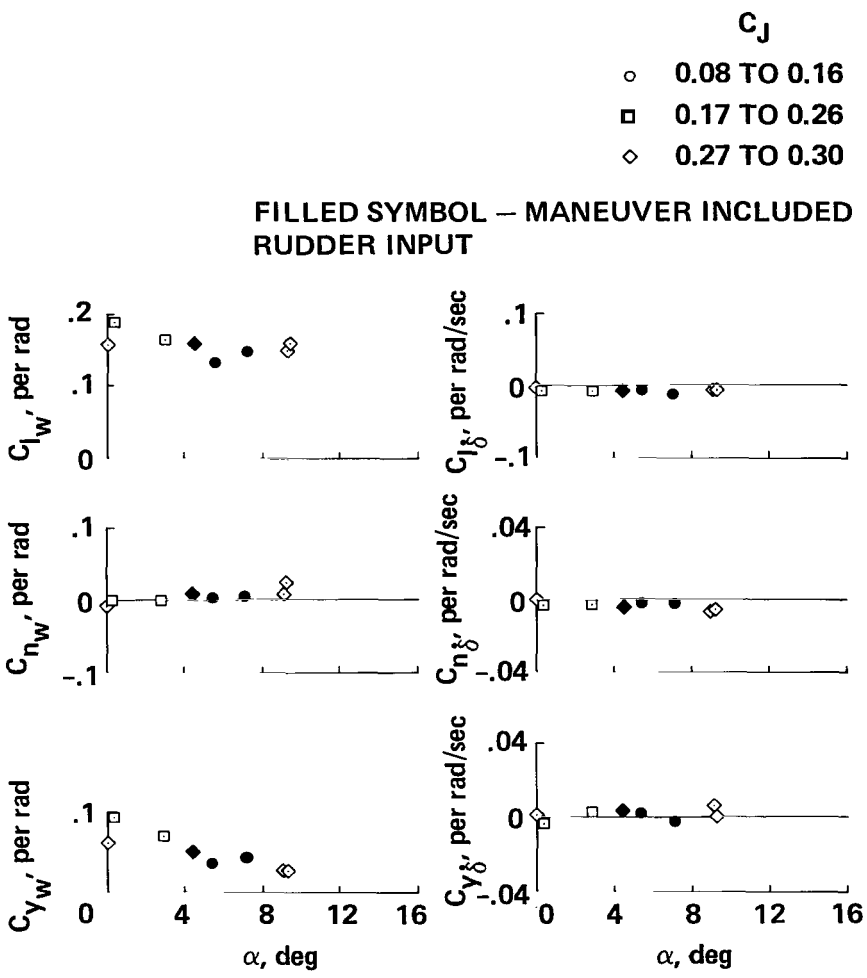

(b) Nozzles at 60°.

Figure 10.- Continued.

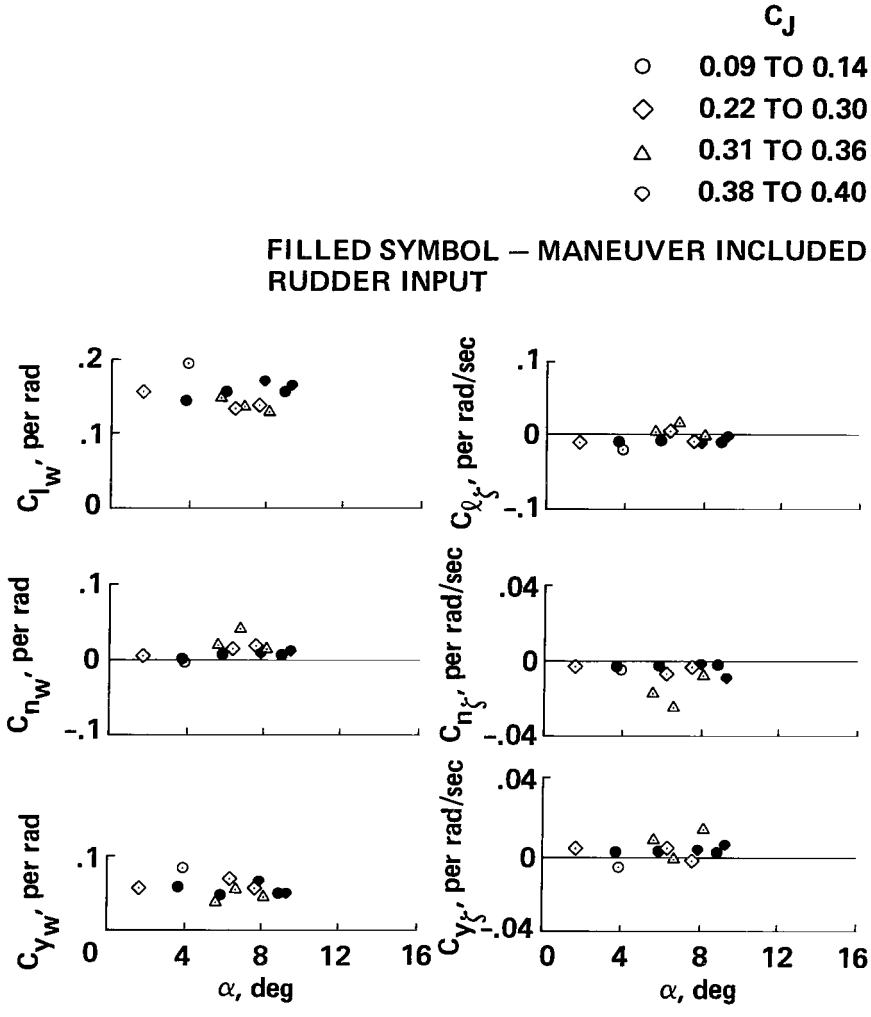

(c) Nozzles at 80° to 90°.

Figure 10.- Concluded.

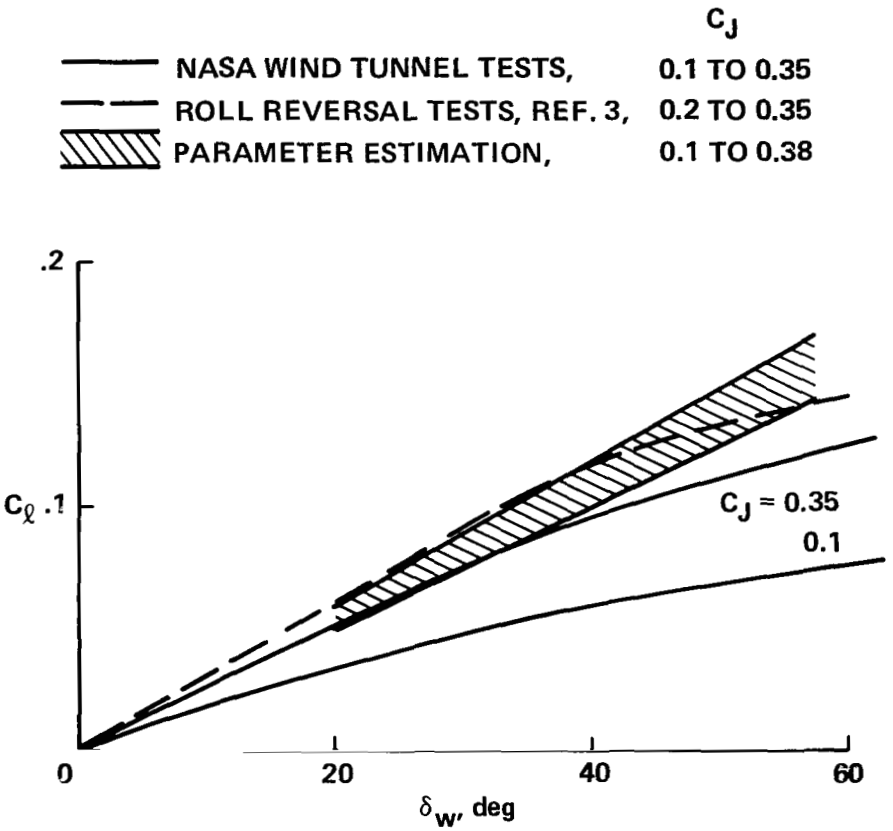

Figure 11.- Rolling moment due to the lateral control vs control-wheel angle.

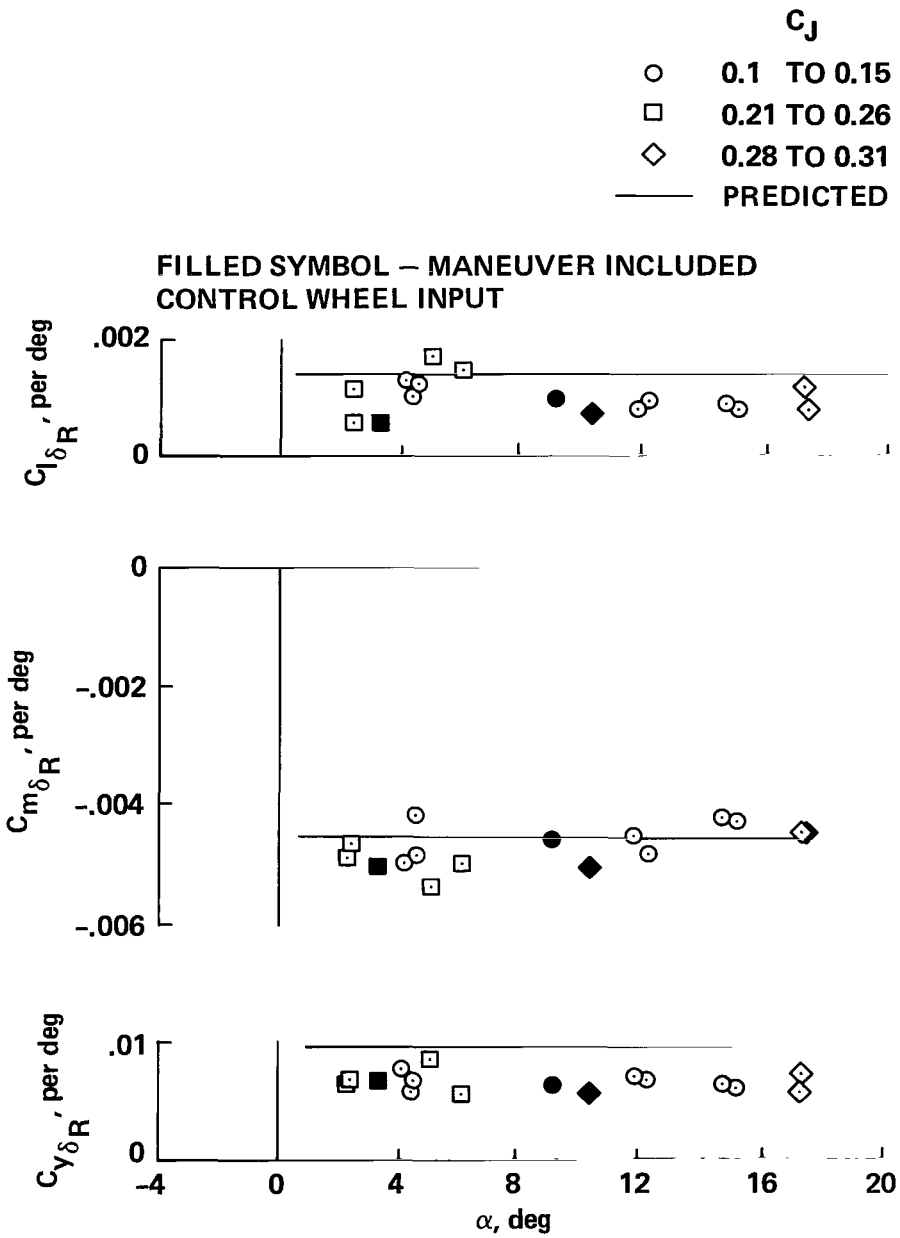

(a) Nozzles at 8°.

Figure 12.- Rudder characteristics.

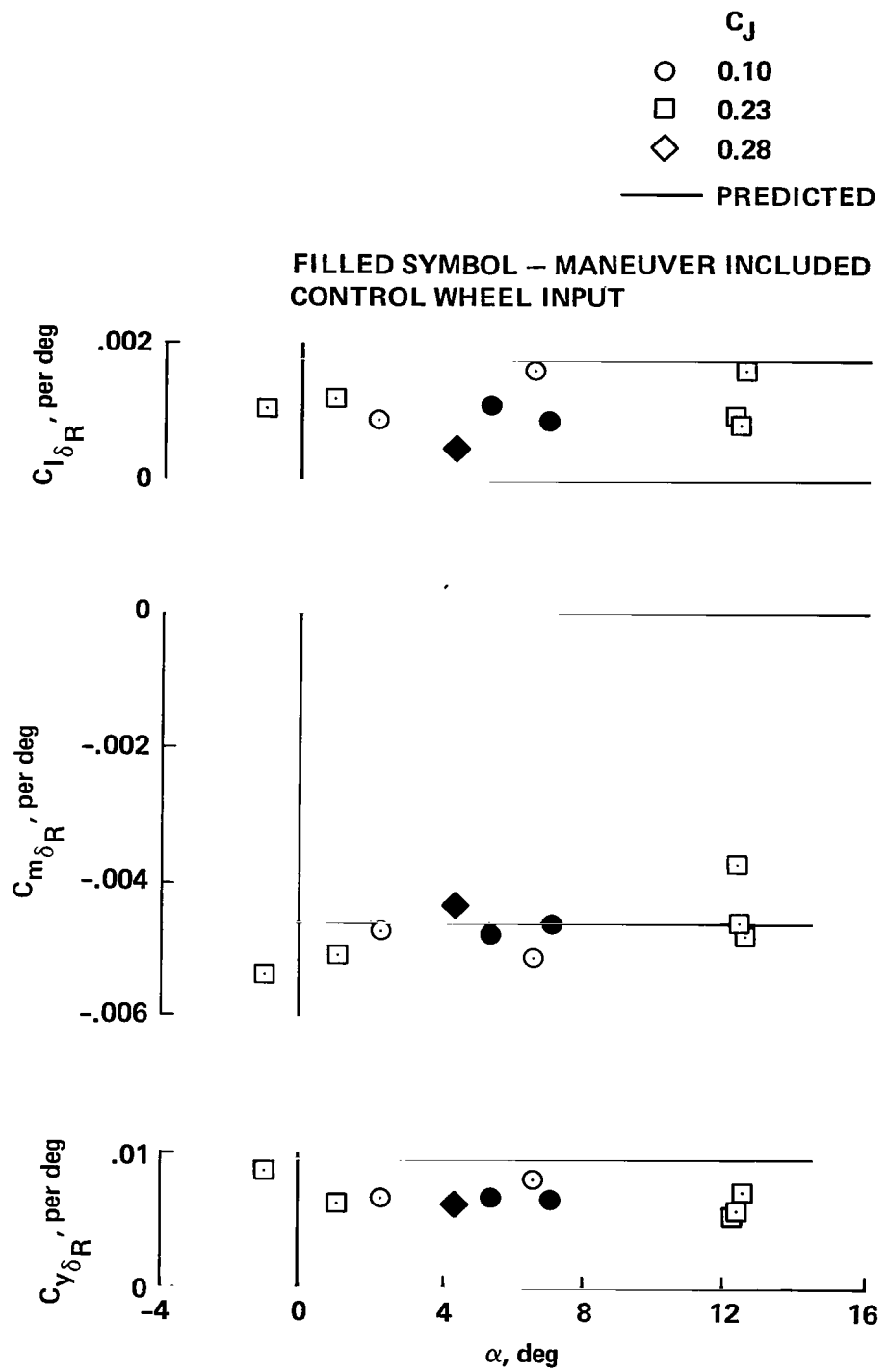

(b) Nozzles at 60°.

Figure 12.- Continued.

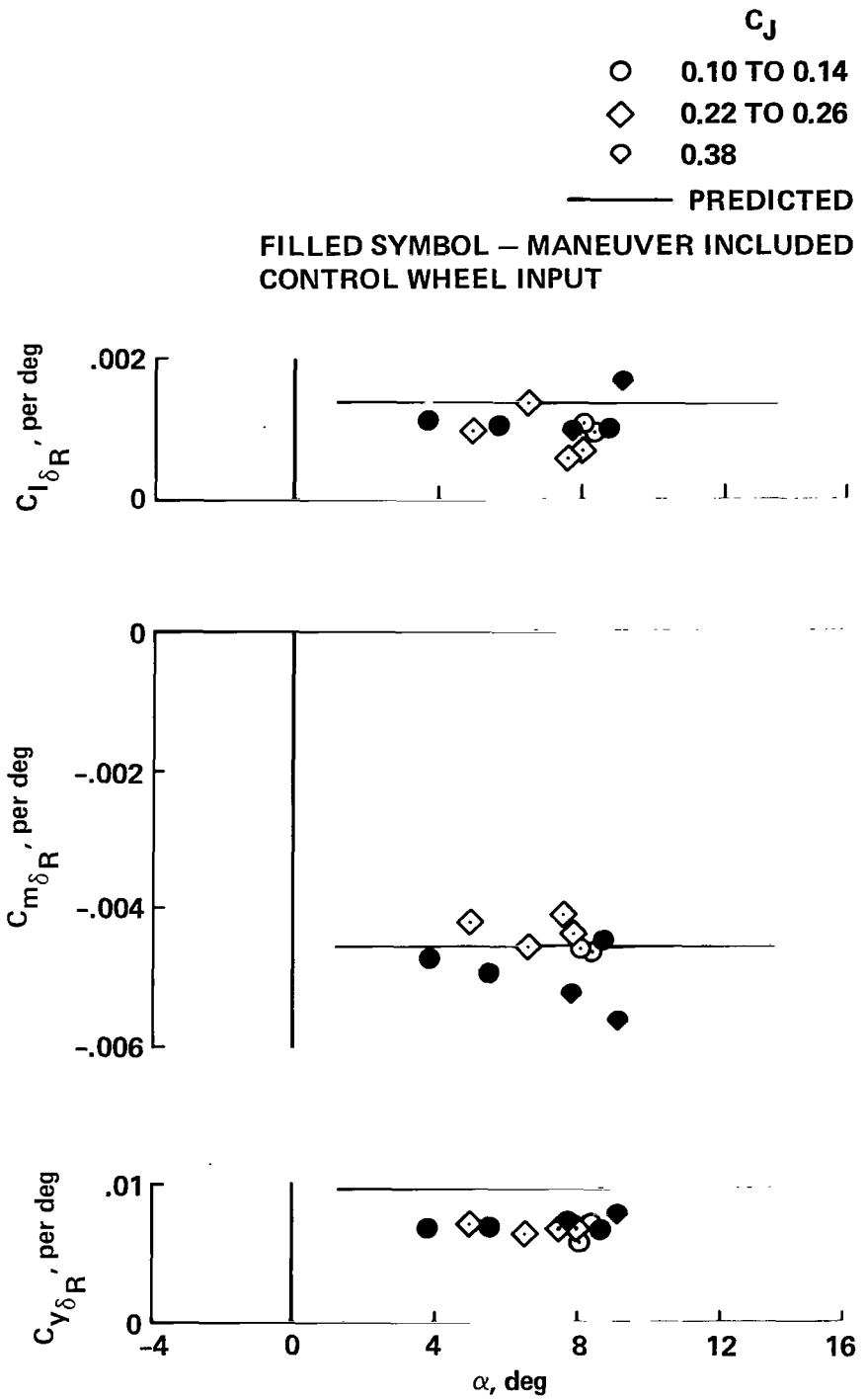

(c) Nozzles at 80° to 90°.

Figure 12.- Concluded.

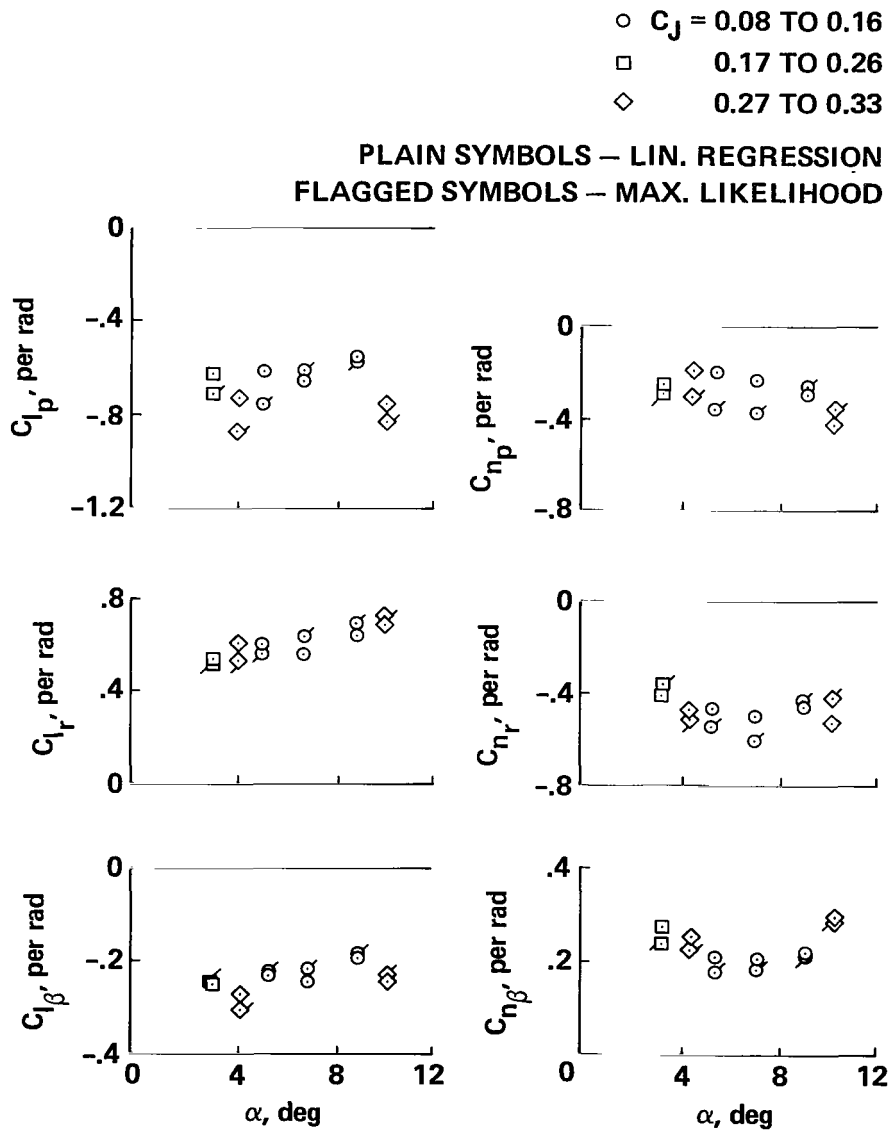

(a) Nozzles angles, 8° and 60°.

Figure 13.- Comparison of derivatives from the maximum-likelihood and the linear-regression solutions.

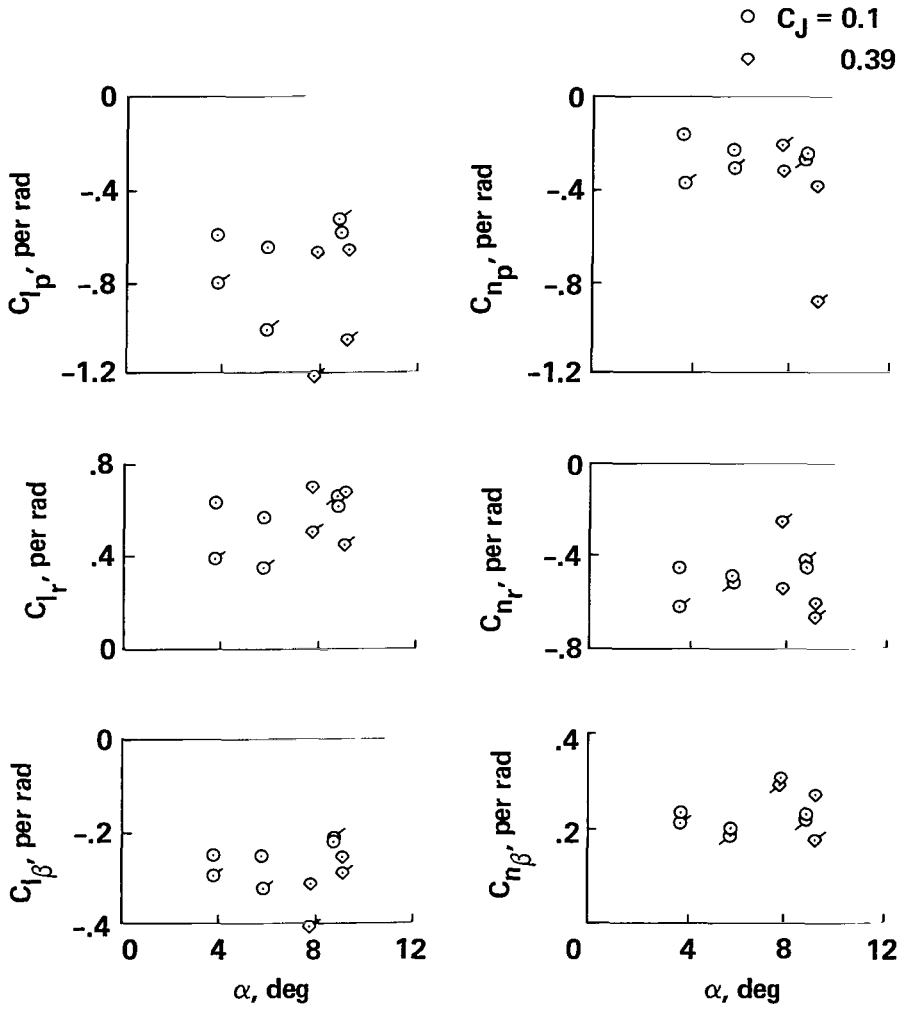

(b) Nozzle angles, 80° to 90°.

Figure 13.- Concluded.

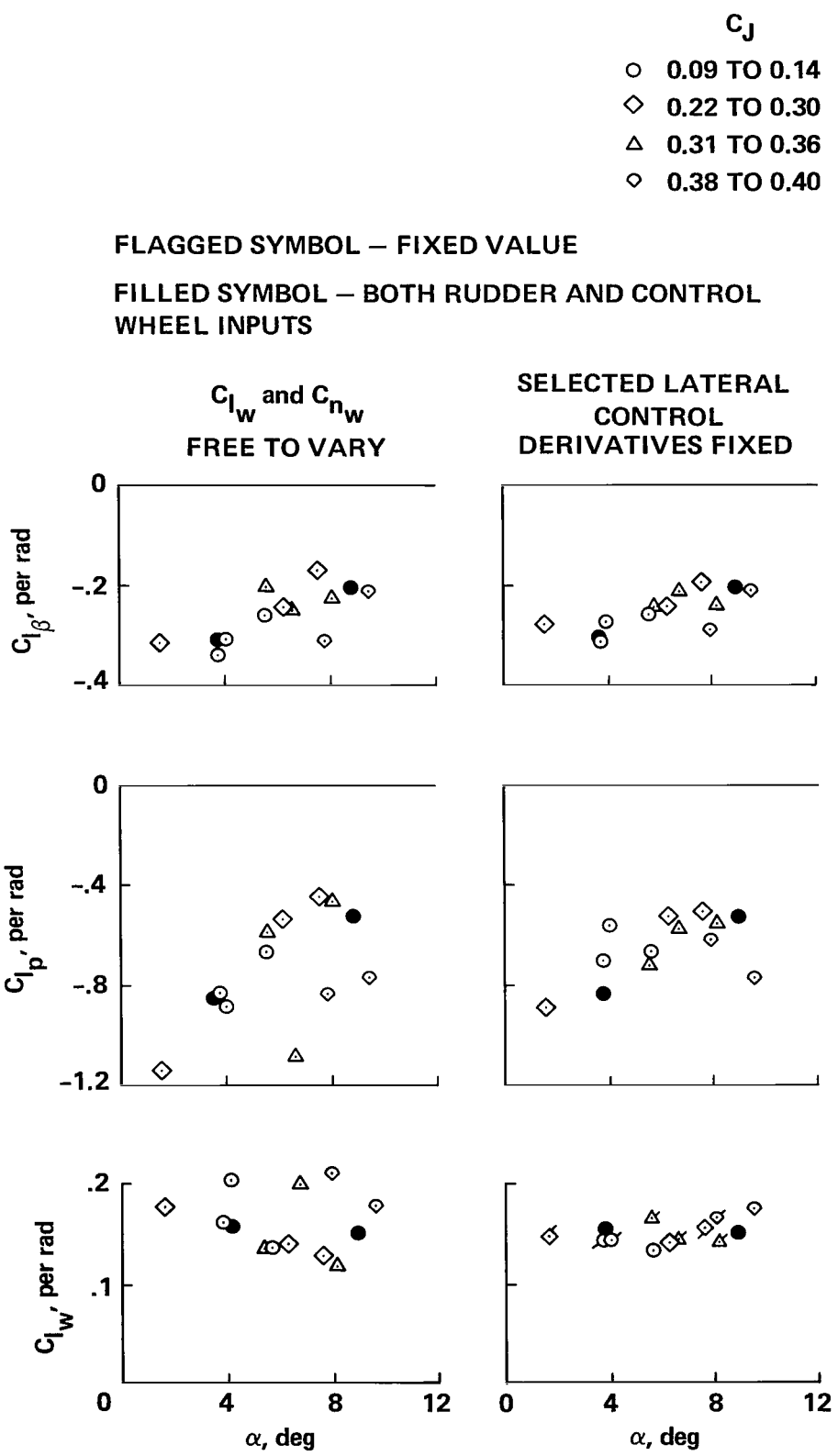

(a) Rolling-moment derivatives.

Figure 14.- Effect on dispersion of setting fixed values for selected lateral-control derivatives: maximum-likelihood solutions; nozzle angles, 80° to 90°.

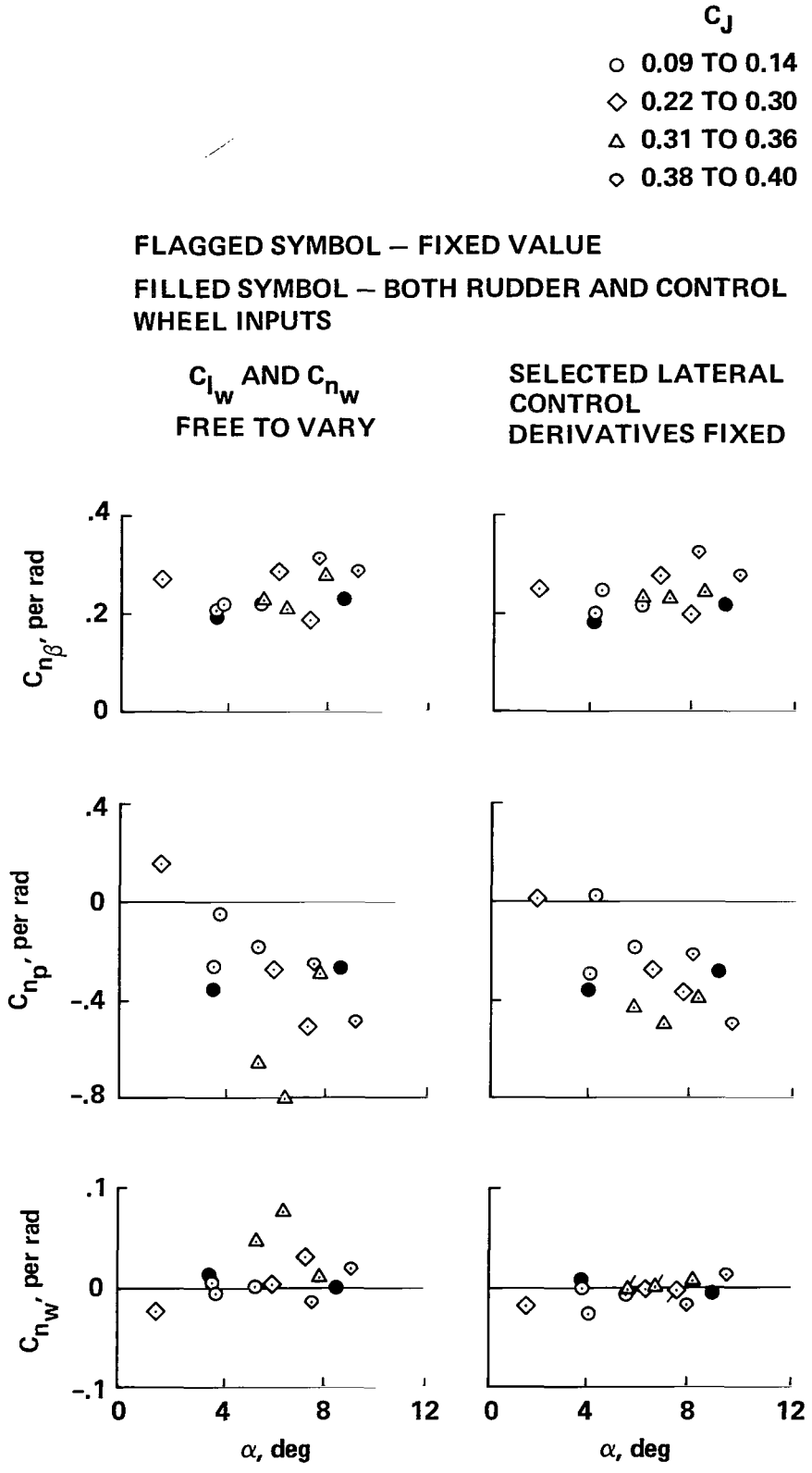

(b) Yawing-moment derivatives.

Figure 14.- Concluded.

1. Report No.	2. Government Accession No.	3. Recipient's Catalog No.
NASA TP-2033		

4. Title and Subtitle
THE APPLICATION OF PARAMETER ESTIMATION TO FLIGHT MEASUREMENTS TO OBTAIN LATERAL-DIRECTIONAL STABILITY DERIVATIVES OF AN AUGMENTED JET-FLAP STOL AIRPLANE

5. Report Date
January 1983

6. Performing Organization Code

7. Author(s)
Jack D. Stephenson

8. Performing Organization Report No.
A-8977

9. Performing Organization Name and Address
NASA Ames Research Center
Moffett Field, Calif. 94035

10. Work Unit No.
T-3478Y

11. Contract or Grant No.

12. Sponsoring Agency Name and Address
National Aeronautics and Space Administration
Washington, D.C. 20546

13. Type of Report and Period Covered
Technical Paper

14. Sponsoring Agency Code
533-02-91

15. Supplementary Notes
Point of Contact: Jack D. Stephenson, Ames Research Center, MS 211-1, Moffett Field, CA, 94035
(415)965-6004 or FTS 448-6004

16. Abstract

Flight experiments with an augmented jet-flap STOL aircraft provided data from which the lateral-directional stability and control derivatives were calculated by applying a linear-regression parameter-estimation procedure. The tests, which were conducted with the jet flaps set at a 65° deflection, covered a large range of angles of attack and engine power settings. The effect of changing the angle of the jet-thrust vector was also investigated. Test results are compared with stability derivatives that had been predicted. The roll damping derived from the tests was significantly larger than had been predicted, whereas the other derivatives were generally in agreement with the predictions. Results obtained using a maximum-likelihood estimation procedure are compared with those from the linear-regression solutions.

17. Key Words (Suggested by Author(s))	18. Distribution Statement
Lateral Stability Stability Derivatives Augmented Jet Flap Airplane Flight Tests	Unclassified - Unlimited Subject Category 08

19. Security Classif. (of this report)	20. Security Classif. (of this page)	21. No. of Pages	22. Price*
Unclassified	Unclassified	62	A04

*For sale by the National Technical Information Service, Springfield, Virginia 22161

NASA-Langley, 1983

National Aeronautics and
Space Administration

Washington, D.C.
20546

THIRD-CLASS BULK RATE

Postage and Fees Paid
National Aeronautics and
Space Administration
NASA-451

Official Busines
Penalty for Priv

S

NASA

POSTMASTER: If Undeliverable (Section 158 Postal Manual) Do Not Return